AFAL-TR-88-086 AD:

Boundary Layer and Singularity Measurement in Three Dimensional Fracture Problems

Final Report
for the period
31 July 1987 to
31 August 1988

October 1988

Authors:
D. Post
C. W. Smith
R. Czarnek

Virginia Polytechnic Institute and
State University
ESM Department
Blacksburg, VA 24061

352-277-1
F04611-87-C-0057

Approved for Public Release

Prepared for the: **Air Force Astronautics Laboratory**

Air Force Space Technology Center
Space Division, Air Force Systems Command
Edwards Air Force Base,
California 93523-5000

NOTICE

When U.S. Government drawings, specifications, or other data are used for any purpose other than a definitely related Government procurement operation, the fact that the Government may have formulated, furnished, or in any way supplied the said drawings, specifications, or other data, is not to be regarded by implication or otherwise, or in any way licensing the holder or any other person or corporation, or conveying any rights or permission to manufacture, use, or sell any patented invention that may be related thereto.

FOREWORD

This final report was submitted by Virginia Polytechnic Institute and State University, Blacksburg, VA on completion of contract F04611-87-C-0057 with the Air Force Astronautics Laboratory (AFAL), Edwards AFB, CA. AFAL Project Manager was Jimmy Liu.

This report has been reviewed and is approved for release and distribution in accordance with the distribution statement on the cover and on the DD Form 1473.

CHI T. LIU
Project Manager

FRANCISCO Q. ROBERTO
Chief, Propellant Development Branch

FOR THE COMMANDER

DAVID P. KING. Lt Col, USAF
Deputy Director
Propulsion Division

SECURITY CLASSIFICATION OF THIS PAGE

REPORT DOCUMENTATION PAGE

Form Approved OMB No. 0704-0188

1a. REPORT SECURITY CLASSIFICATION: UNCLASSIFIED	1b. RESTRICTIVE MARKINGS
2a. SECURITY CLASSIFICATION AUTHORITY	3. DISTRIBUTION/AVAILABILITY OF REPORT: Approved for public release; distribution is unlimited.
2b. DECLASSIFICATION/DOWNGRADING SCHEDULE	
4. PERFORMING ORGANIZATION REPORT NUMBER(S): 352-277-1	5. MONITORING ORGANIZATION REPORT NUMBER(S): AFAL-TR-88-086
6a. NAME OF PERFORMING ORGANIZATION: Virginia Polytechnic Inst. and State University; 6b. OFFICE SYMBOL (If applicable)	7a. NAME OF MONITORING ORGANIZATION: Air Force Astronautics Laboratory
6c. ADDRESS (City, State, and ZIP Code): ESM Department - VPI&SU, Blacksburg, VA 24061	7b. ADDRESS (City, State, and ZIP Code): RKPL, Edwards AFB CA 93523-5000
8a. NAME OF FUNDING/SPONSORING ORGANIZATION; 8b. OFFICE SYMBOL (If applicable)	9. PROCUREMENT INSTRUMENT IDENTIFICATION NUMBER: F04611-87-C-0057
8c. ADDRESS (City, State, and ZIP Code)	10. SOURCE OF FUNDING NUMBERS: PROGRAM ELEMENT NO.; PROJECT NO. 2302; TASK NO M1; WORK UNIT ACCESSION NO. 8L

11. TITLE (Include Security Classification)
Boundary Layer and Singularity Measurement in Three Dimensional Fracture Problems (U)

12. PERSONAL AUTHOR(S)
Post, D., Smith, C. W., and Czarnek, R.

13a. TYPE OF REPORT	13b. TIME COVERED	14. DATE OF REPORT (Year, Month, Day)	15. PAGE COUNT
Final	FROM 87/7/31 TO 88/8/31	88/10	

16. SUPPLEMENTARY NOTATION

17. COSATI CODES			18. SUBJECT TERMS (Continue on reverse if necessary and identify by block number)
FIELD	GROUP	SUB-GROUP	Crack Opening; Crack Growth; Inert Propellant, Pure Binder; Near Tip Displacement; Strain Determination; Dominant Singularity Order Distribution.

19. ABSTRACT (Continue on reverse if necessary and identify by block number)

Experimental methods (coarse grid and high density moire interferometry) were used to measure near tip surface displacement during the opening and growth of cracks in "biaxial" specimens of inert propellant and pure binder in tests conducted at two different head rates (2.5 and 25.4 mm/min). Displacement data were collected from coarse grids at regular time intervals. An intense strain zone developed ahead of the crack tip in both materials. However, the size of the zone in the inert propellant was at least an order of magnitude larger than in the pure binder, shifting the high strain contours ahead of the crack tip. From such data, an idealized model for the intense strain zone in the inert propellant was postulated.

Values of the dominant eigenvalue near the crack tip were computed from appropriate algorithms where the crack intersected the free surface. Frozen stress photoelastic analysis of four point bend tests were used to infer the distribution of the dominant eigenvalue through the specimen thickness for both straight front and thumbnailed cracks.

20. DISTRIBUTION/AVAILABILITY OF ABSTRACT: ☒ UNCLASSIFIED/UNLIMITED ☐ SAME AS RPT ☐ DTIC USERS	21. ABSTRACT SECURITY CLASSIFICATION: UNCLASSIFIED
22a. NAME OF RESPONSIBLE INDIVIDUAL: Chi T. Liu	22b. TELEPHONE (Include Area Code): (805) 275-5274; 22c. OFFICE SYMBOL: RKPL

DD Form 1473, JUN 86 — Previous editions are obsolete. — SECURITY CLASSIFICATION OF THIS PAGE

Block 19 (concluded): Results compared favorably with an analytical result obtained by Benthem.

Results indicate an absence of transverse constraint in the intense strain zone of the inert propellant which suggests the absence of a strong thickness effect upon the threshold value of the stress intensity factor.

TABLE OF CONTENTS

LIST OF FIGURES

INTRODUCTION

As performance requirements for rocket motors are advanced, it becomes increasingly important to understand and control the influence of defects in the motor grain. One of the most potentially serious types of defects are cracks which may occur during curing or later in storage. These cracks may act as thermal insulators and may significantly alter subsequent motor performance. Attempts to develop and validate mathematical models for predicting behavior of such cracks in motor grain have been hampered by lack of an extensive data base and lack of quantification of three dimensional effects.

In a recent study [Ref. 1], some progress was made towards development of a data base for understanding the near tip behavior of cracks in inert propellant samples. These studies revealed that a significant amount of severe blunting developed at the crack tip prior to crack extension but that, in the early stages of crack opening, a reduction in the order of the stress singularity occured when the crack intersected the free surface of the inert propellant, and this reduction was accurately measured at the free surface by a grid method which did not influence the near tip behavior. The variation in the stress singularity order with direction normal to the free surface was then studied using four point bend frozen stress photoelastic specimens.

All of the above studies were conducted on "artificial" or man-made straight front cracks and seemed to indicate that the binder, though only present in small volume fraction, controlled the near tip process.

Since it is well known that through cracks "thumbnail" when they grow in plates of continua such as metals and plastics under Mode I loading, and that this changes the boundary intersection angle between the crack front and the free surface of the specimen, the question arose as to what the effect of thumbnailing would be upon the free surface singularity order, its distribution through the thickness and the near tip displacement and strain fields. Also at issue was the influence of a surface layer of binder on specimens of inert propellant tested and reported on in Ref. 1. In order to clarify these issues, the following program was developed and conducted.

PROGRAM OBJECTIVES

The objectives of the present program were:

To measure the components of the displacement field in the free surface of specimens, at intervals of time during constant head rate separations producing extension of the crack in "biaxial" specimens of inert propellant without surface layers of binder and specimens of pure binder and extract surface strain distributions from the data.

To estimate the order of the stress singularity or dominant eigenvalue for the crack at the free surface for a growing crack and to study the crack front shape and its influence thereon.

PROGRAM SCOPE

The program consisted of three phases: 1) Fabrication of cracked biaxial specimens of both inert propellant and pure binder (with additives), 2) Measurement of displacement fields near crack tips and determination of near tip strain fields and singularity order at the free surface for grown cracks along with measurement of crack front shapes for both inert propellant and pure binder. Determine singularity order distribution through thickness using the frozen stress method on a four point bend specimen for naturally grown "thumbnailed" cracks. 3) Preparation of a final comprehensive technical report describing the results of the effort.

WORK PLAN AND ACCOMPLISHMENTS

The program conducted can be conveniently separated into two parts:

1) Mode I constant head rate tests on "biaxial" cracked specimens of pure binder and inert propellant with measurements of surface displacements and crack front shapes during growth followed by extraction of near tip strain fields and the free surface stress singularity or dominant eigenvalue order, and 2) Frozen stress tests on four point bend specimens containing thumbnailed natural crack fronts to measure variation of the lowest dominant eigenvalue with direction normal to the free surface.

BIAXIAL TESTS; METHODS, MEASUREMENTS AND RESULTS

Preliminary tensile tests on the pure binder yielded a value of Elastic Modulus E = 112.3 psi = 0.776 MPa and Poisson's Ratio $\nu \approx 0.47$ at room temperature below a nominal global strain ($\bar{\varepsilon}_y$) of $\approx$ 20%.

The "biaxial" test specimen configuration is pictured in Figure I and is the same as employed in Ref. 1. The pure binder material consisted of polybutadiene rubber with chemical additives used to enhance its capability to bond to propellant particles. It was manufactured by Morton Thiokol under the name R45M Gumstock. The inert propellant consisted of this binder with embedded polyhedral particles of potassium chloride, the latter occupying a volume fraction of approximately 75%. The particle sizes ranged from .01 to 0.5 mm. The inert propellant was also supplied by Morton Thiokol under the name H-24 inert propellant.

A grating consisting of squares 0.2 mm on a side was applied to the inert propellant specimen using the following procedure:

- Spread titanium dioxide powder over the specimen surface near the crack tip.
- Apply a mixture of silicone grease and titanium dioxide to the surface.
- Place a metal screen in the surface mixture and remove excess mixture.

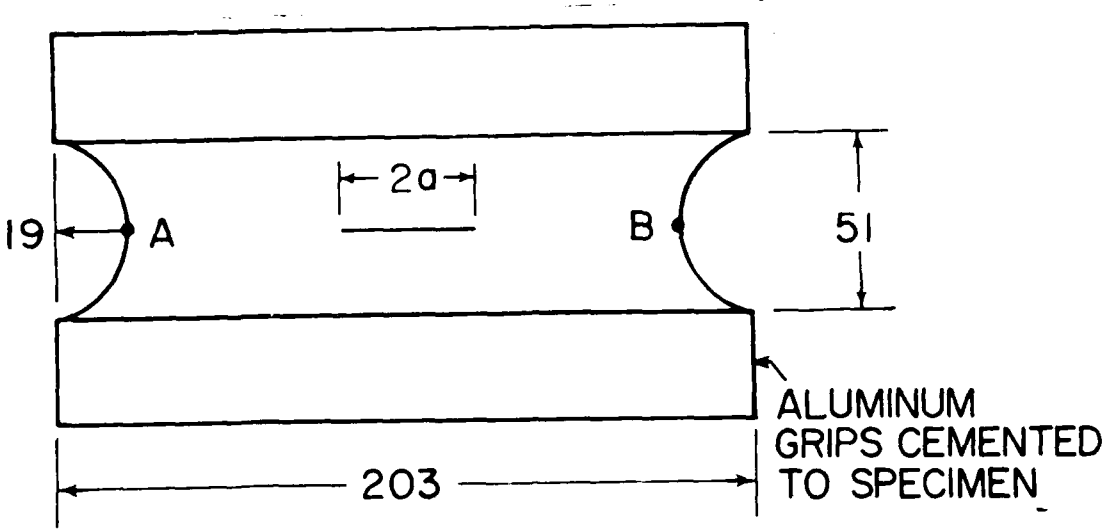

DIMENSIONS IN MILLIMETERS: Initial Crack Length (2a) ~38 mm
Specimen thickness = 15.25 mm

Fig. 1 Biaxial Test Specimen Dimensions

- Evaporate aluminum over the screened surface.
- Remove the metal screen.

The same size grating was produced on the binder using the following procedure:

- Apply a special adhesive to the binder surface.
- Place a metal screen on it.
- Evaporate aluminum on this surface.
- Remove the metal screen as before.

The total thickness of the resulting grating was less than 2.5×10^{-2} mm.

Tests were conducted at constant head rates of 2.5 mm/min and at 25.4 mm/min and photographs of the grid region were taken at various time intervals. A schematic of the photographic setup is shown in Figure 2. The lighting provided by the ring illuminator and reflector was critical. Figure 3 shows typical load-extension-time records for tests on both propellant and pure binder at each rate showing both the strengthening and stiffening effect of the rigid particles. Figure 4 illustrates a typical set of raw data for an inert propellant test and a pure binder test illustrating the processes involved in crack extension. At a given instant during crack growth, a dark powder was "shot" into the crack opening to mark the crack front shape. A summary of the

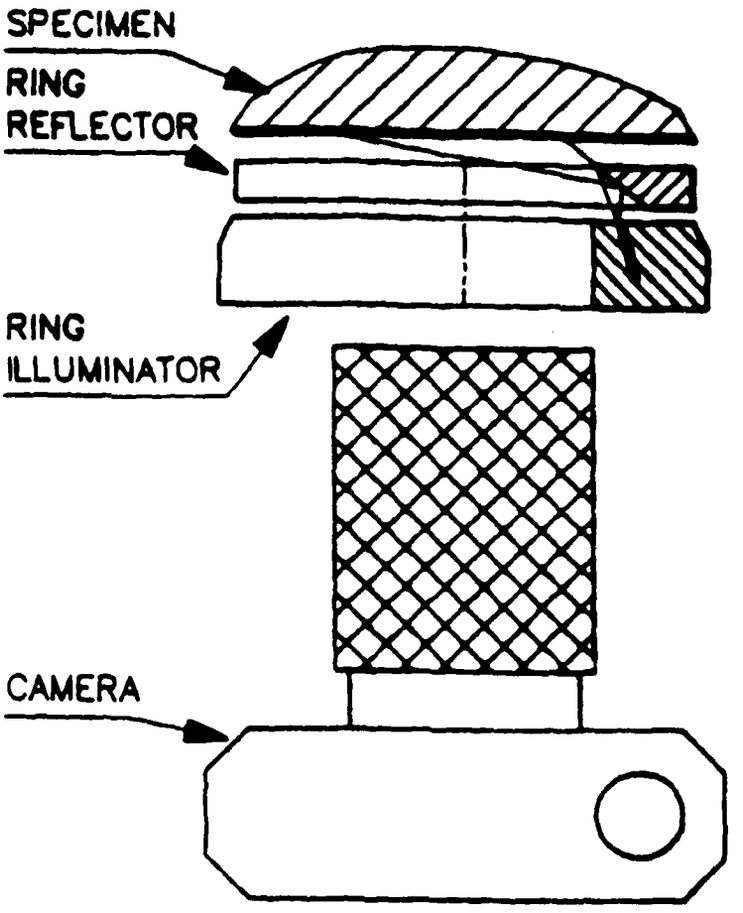

Fig. 2 Schematic of Photographic Setup

biaxial tests conducted and the corresponding head rates and dominant eigenvalue data zones are given in Table I.

Data from photographs such as those in Figure 4 were digitized and displacement and strain fields were extracted following the procedures of Ref. 1 (Appendix A). Typical results are shown in Figure 5. Examination of results revealed that the effect of changing the head rate by an order of magnitude altered the displacement fields (and also the strain fields) but the distribution contours were of the same general form. Consequently, we shall present digitized data here only for the slow rate. Figure 5 presents a complete set of digitized results, (U, V, ε_x, ε_y, γ_{xy}) for a global strain level of $\bar{\varepsilon}_y$ = 4% from an inert propellant (IP) test (Figs. 5a through 5e) and a set for a global strain level of $\bar{\varepsilon}_y$ = 4.7% from a pure binder (PB) test (Figs. 5f through 5j) for purposes of comparison. Comparing the displacement fields in Figs. 5a and 5b with those in Figs. 5f and 5g, respectively, we find similar global contour shapes. In determining ε_x and ε_y, data were averaged from the two sides of the crack plane to eliminate any possible in-plane shear mode effect.

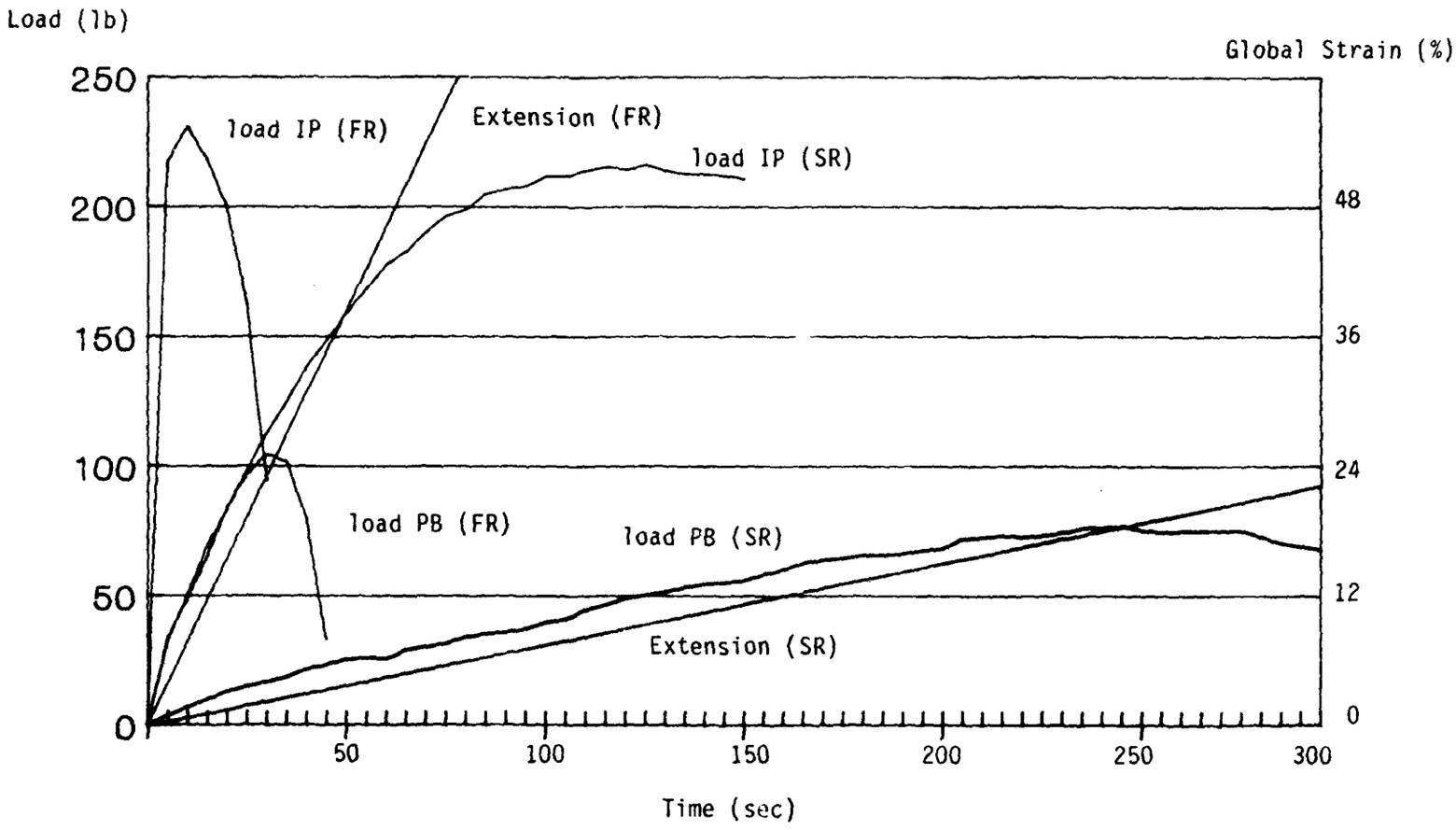

SR (slow head rate) - 2.5 mm/min

FR (fast head rate) - 25.4 mm/min

Fig. 3 Load-Extension-Time Records - Inert Propellant (IP) and Pure Binder (PB)

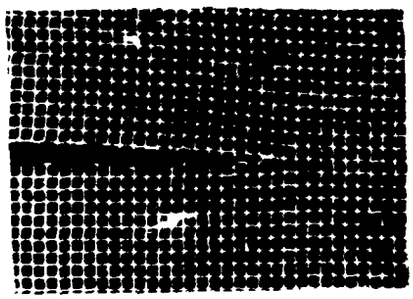

(a) $\bar{\varepsilon}_y$ = 0.76%

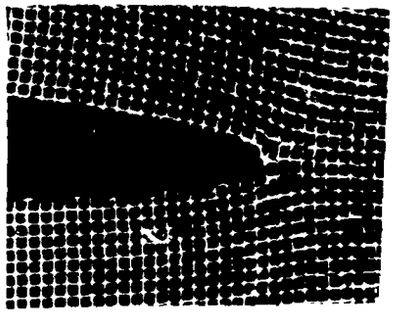

(b) $\bar{\varepsilon}_y$ = 3.95%

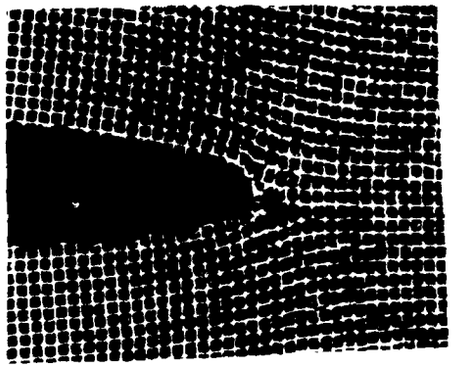

(c) $\bar{\varepsilon}_y$ = 4.76%

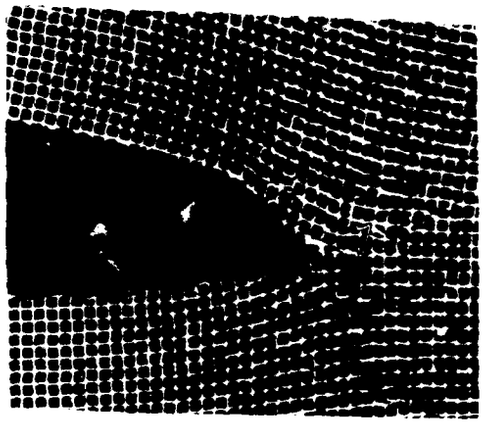

(d) $\bar{\varepsilon}_y$ = 6.05%

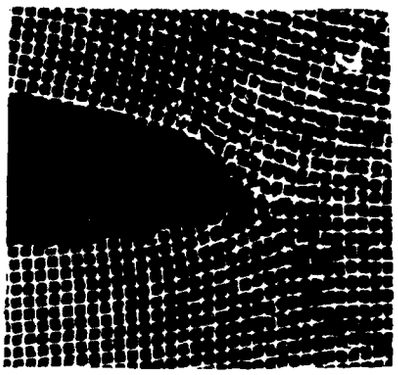

(e) $\bar{\varepsilon}_y$ = 6.45%

TEST P2

HEAD RATE: 2.5 mm/min

M.F. = 8.73

Fig. 4 Crack Opening and Growth in Specimen P-2
a) Opening b) Blunting c) Void Formation
d) Coalesence of Void with Main Crack
e) Crack Extension

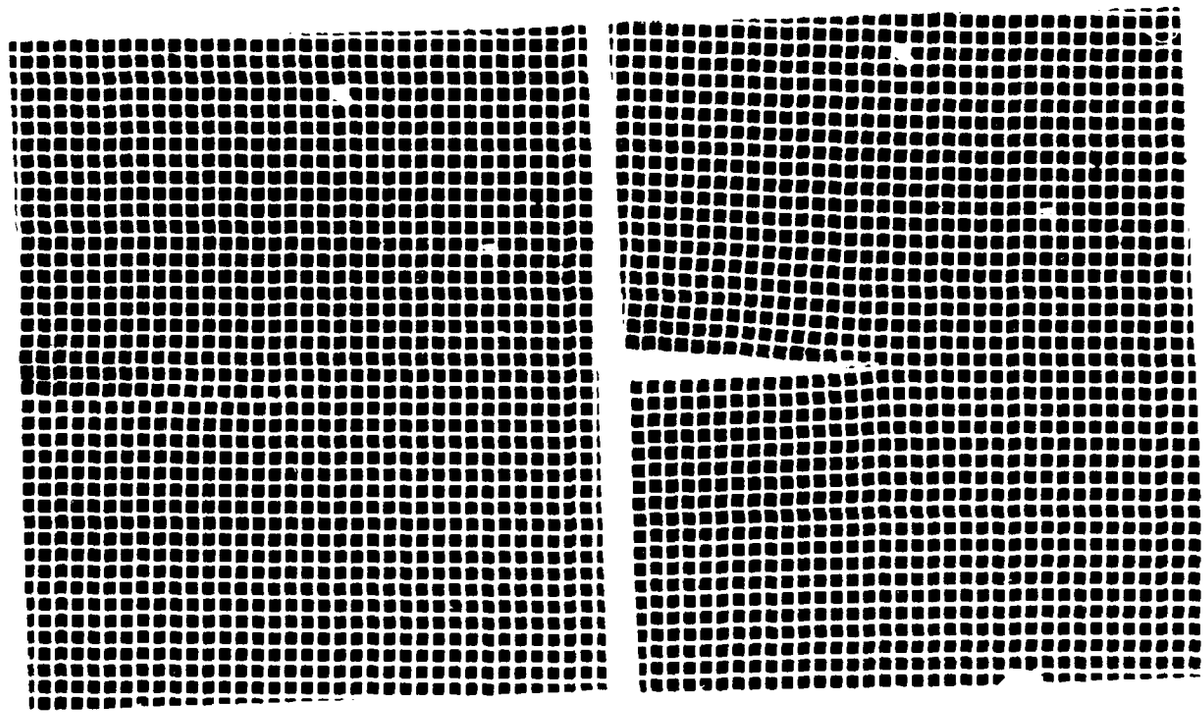

(f) $\bar{\varepsilon}_y$ = 0%

(g) $\bar{\varepsilon}_y$ = 1.93%

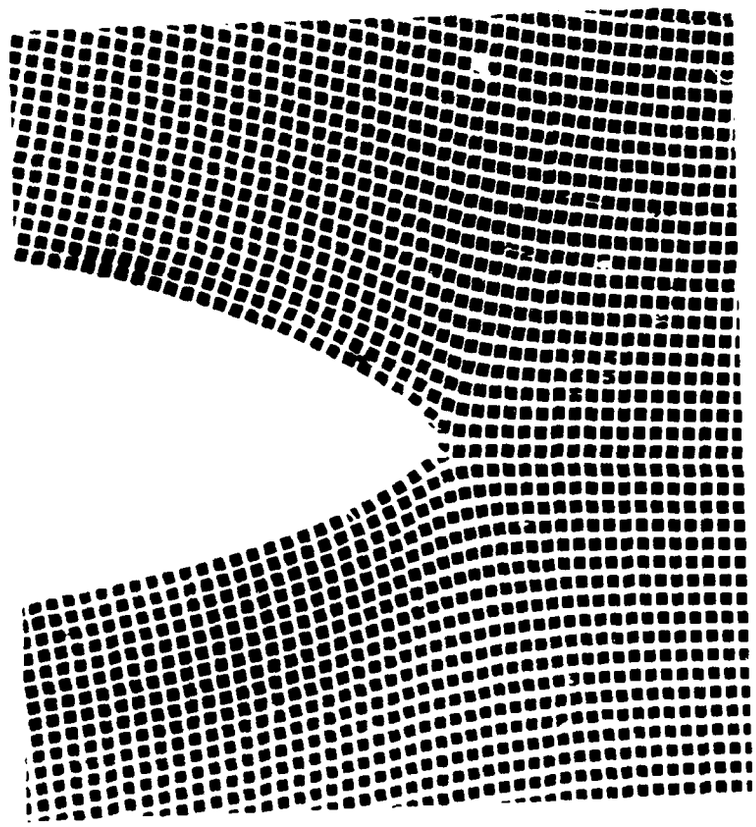

(h) ε_y = 11.30%

TEST B-2
HEAD RATE = 2.5 mm/min
M.F. = 11.6

Fig. 4 Crack Opening and Growth in Specimen B-4
(f) No Load
(g) Opening
(h) Growth

TABLE 1

Uniaxial Test Data for K_u Determination

Grating Frequency 52/mm

Test No.	Head Rate mm/min	Data Zone for K_u Det. mm
	Inert Propellant	
P-1	2.5	3.5-5.0
P-2	2.5	1.5-5.0
P-3	25.4	1.5-4.5
P-4	25.4	1.5-5.0
	Pure Binder	
B-1	2.5	1.0-6.0
B-2	2.5	1.5-5.0
B-3	25.4	1.0-6.0
B-4	25.4	1.5-5.0
B-5	2.5	1.5-5.0
B-6	2.5	1.5-5.0

Computer plots of the strain distributions ε_x, ε_y, γ_{xy} for the IP in Figs. 5c through 5e may be compared with those from the PB in Figs. 5h through 5j. The approximate location of the opened crack has been sketched in for purposes of orientation. Moreover, strain contours for strain levels greater than 15% should be ignored since small strain definitions were used here.

The strain contours are generally more irregular (especially the shear strain ones) for the IP than for the PB and that was expected due to the presence of the rigid particles in the IP. However, some irregularities are seen in the PB strain contours as well which may be inherent in the digitizing process.

Focusing upon a comparison of the ε_y contours, we note that the intense strain zone ahead of the blunted crack in the IP (Fig. 5d) tends to increase the strain levels surrounding that zone above those in the PB (Fig. 5i) especially in the direction of crack extension. A similar conclusion is reached in comparing Figs. 5e and 5j for the shear strain contours γ_{xy}. This suggests that any mathematical model which is used to describe the strain fields surrounding the near tip intense strain zone should reflect the presence of that zone. The computer plot of the ε_y contours in Fig. 5i for the PB also shows an intense strain field very near the crack tip, but it is at least an order of magnitude smaller in size than in the IP. On the other hand, the larger crack opening in the PB and the near tip blunting in the IP both seem to distribute the near tip shear strain intensity (Figs. 5e and 5j) over the enlarged tip. ε_x, of course, vanishes due to symmetry at the crack tip on the crack plane.

Test	P2
Near Tip Field of Digitized Interval	U 0.05 mm
Head Rate	2.5 mm/min
Global Strain $\bar{\varepsilon}_y$	4.0 %

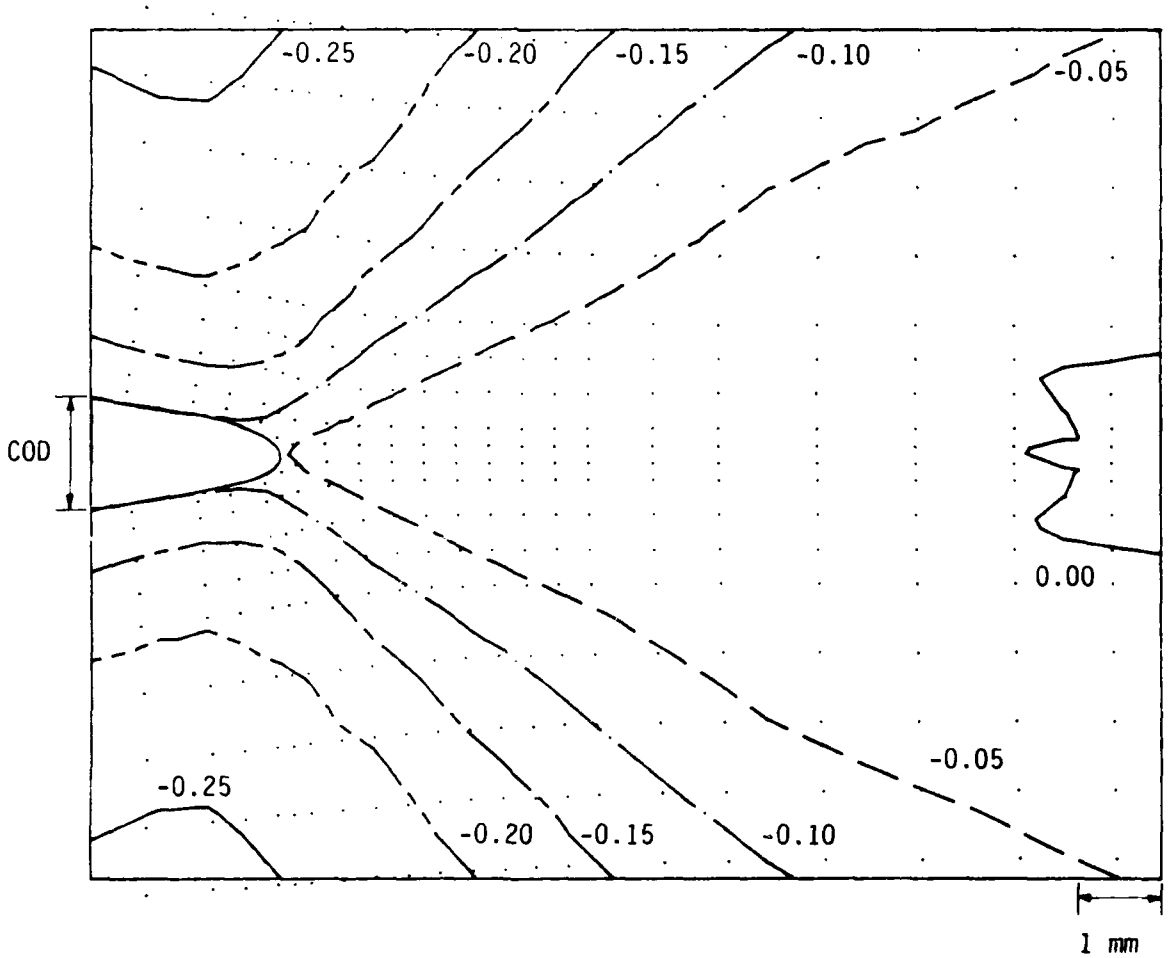

Fig. 5 a) U Displacement Field, Slow Rate, IP

Test	P2
Near Tip Field of Digitized Interval	V 0.1 mm
Head Rate	2.5 mm/min
Global Strain $\bar{\varepsilon}_y$	4.0 %

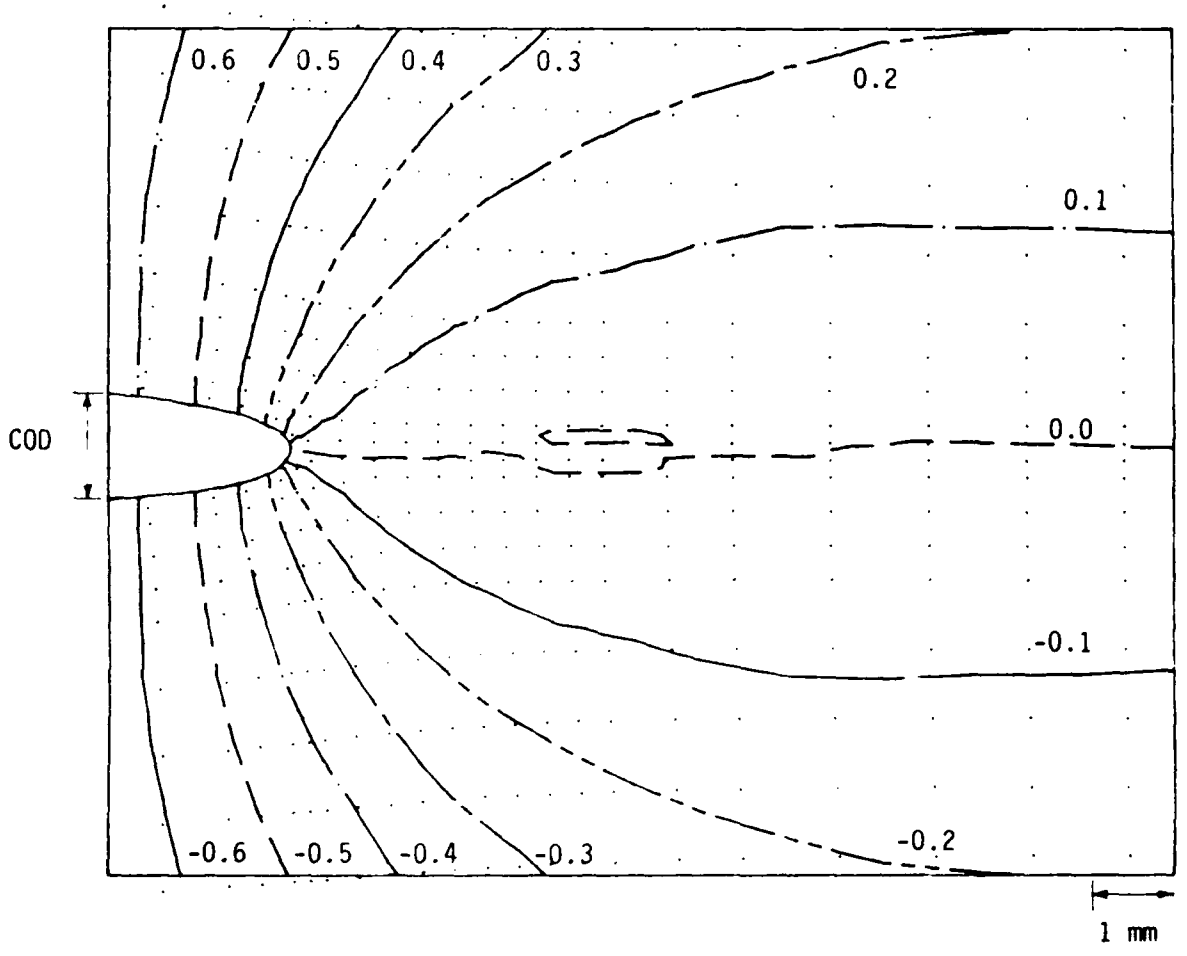

Fig. 5 b) V Displacement Field, Slow Rate, IP

Test	P2
Near Tip Field of Digitized Interval	ε_x 0.05
Head Rate	2.5 mm/min
Global Strain $\bar{\varepsilon}_y$	4.0%

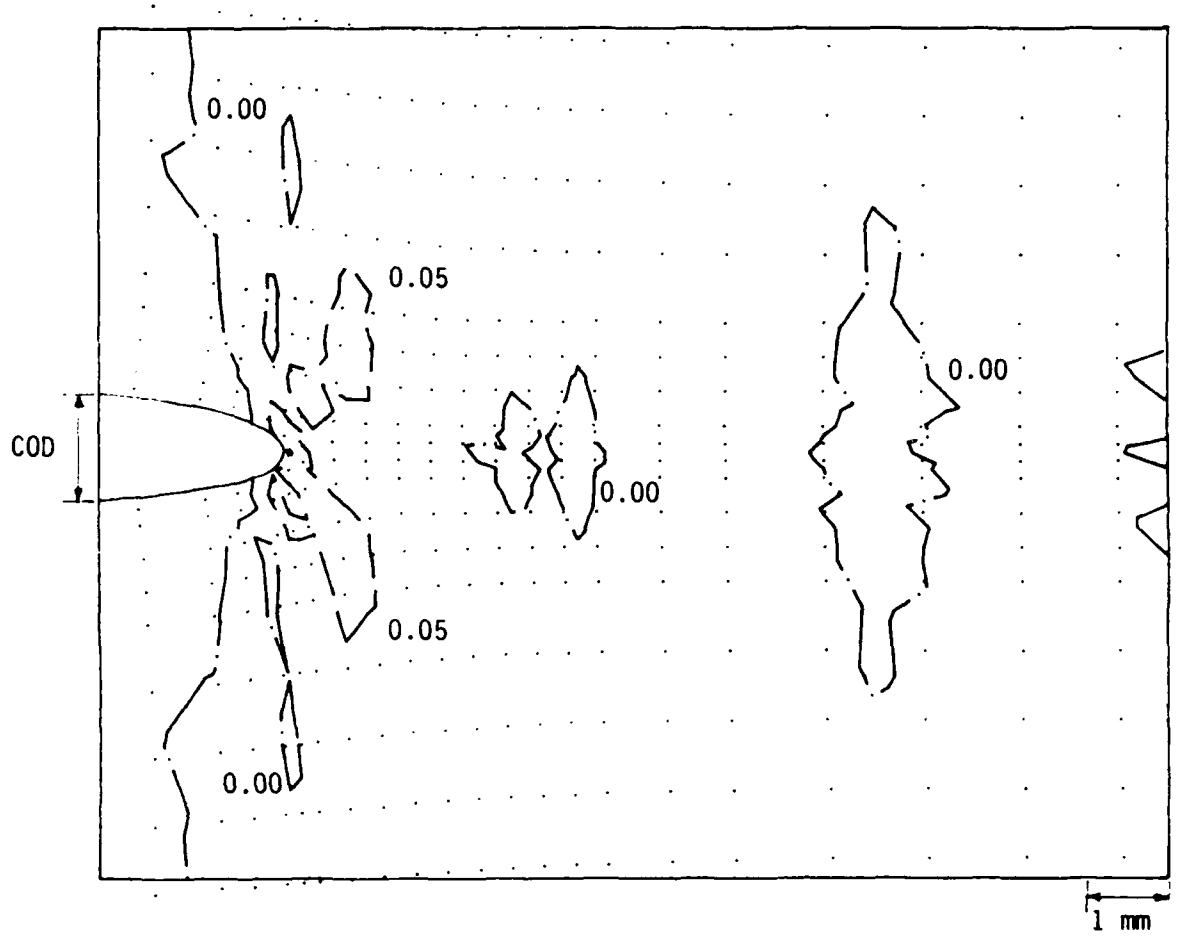

Fig. 5 c) ε_x Slow Rate, IP

Test	P2
Near Tip Field of Digitized Interval	ε_y 0.05
Head Rate	2.5 mm/min
Global Strain $\bar{\varepsilon}_y$	4.0%

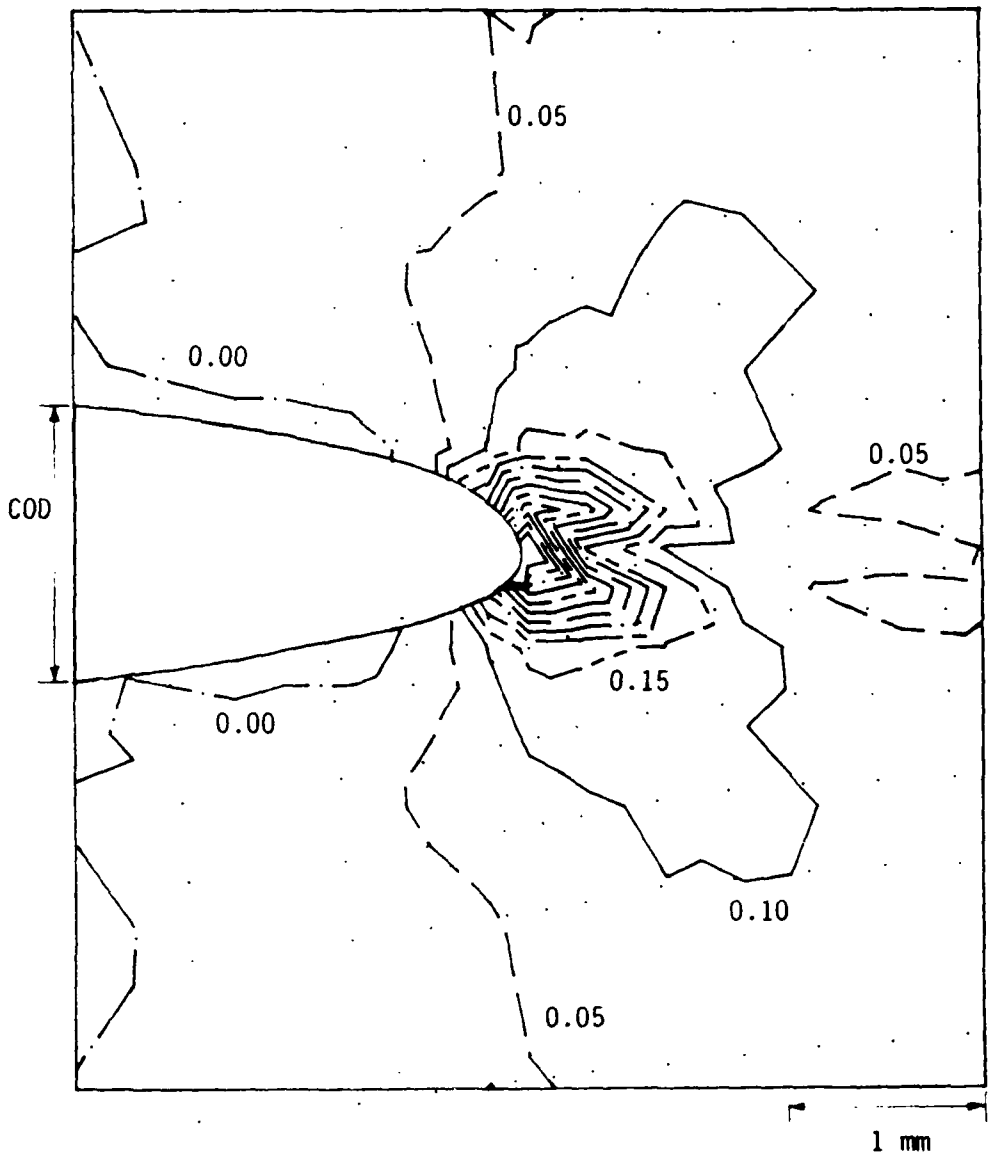

Fig. 5 d) ε_y Slow Rate, IP

Test	P2
Near Tip Field of Digitized Interval	γ_{xy} 0.05
Head Rate	2.5 mm/min
Global Strain $\bar{\varepsilon}_y$	4.0%

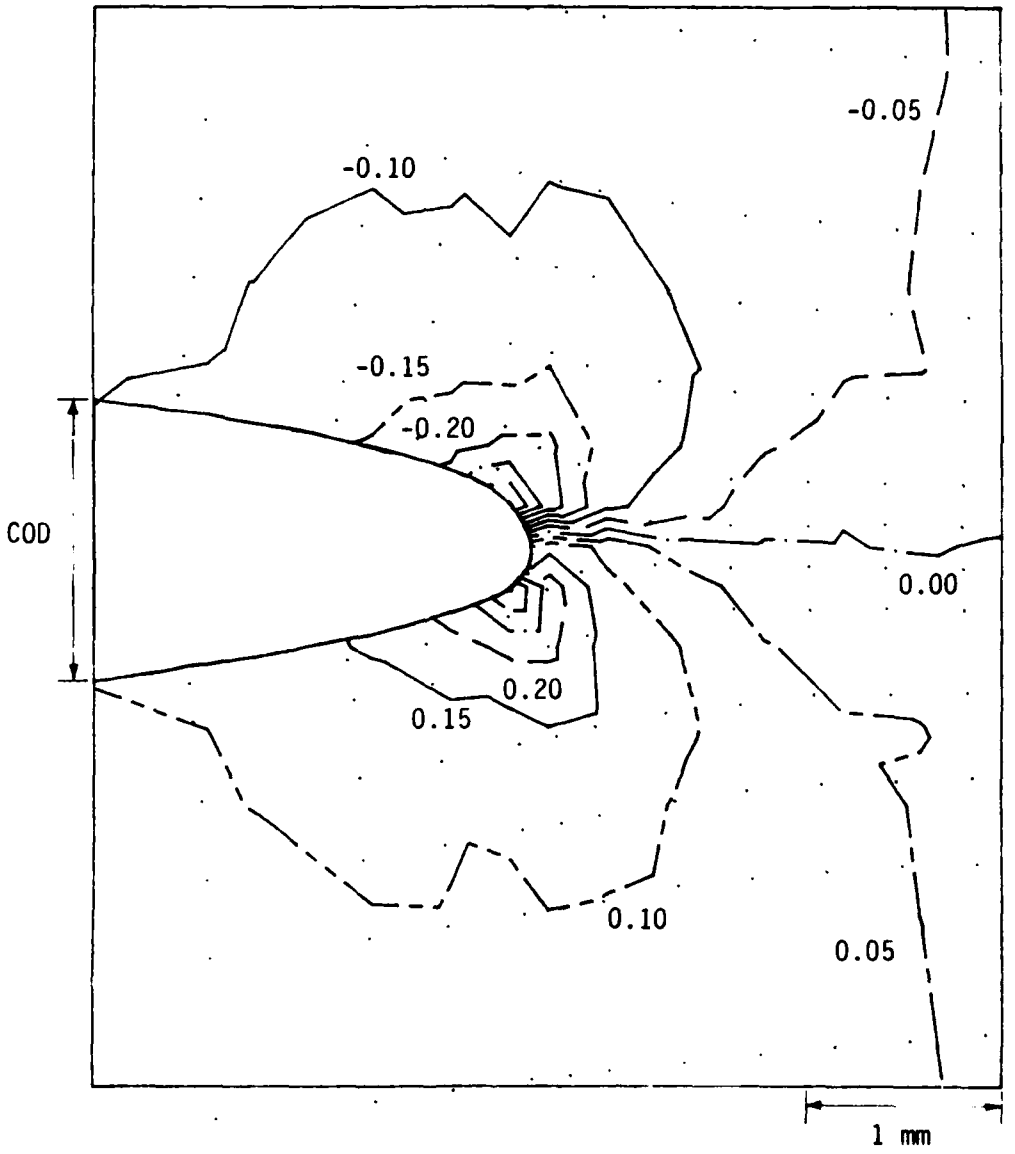

Fig. 5 e) γ_{xy} Slow Rate, IP

Test	B5
Near Tip Field of Digitized Interval	U 0.05 mm
Head Rate	2.5 mm/min
Global Strain $\bar{\varepsilon}_y$	4.7%

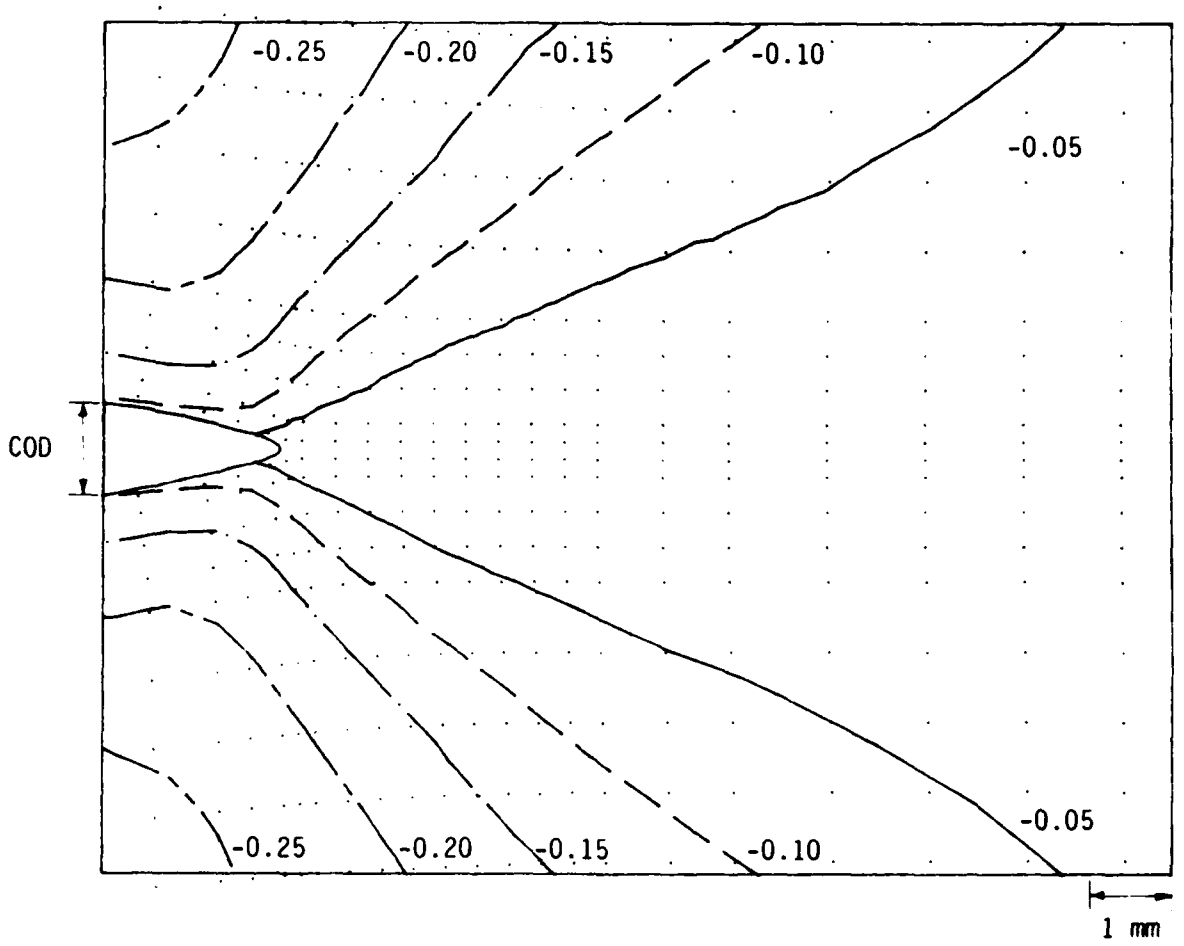

Fig. 5 f) U Displacement Field,Slow Rate, PB

Test	B5
Near Tip Field of Digitized Interval	V 0.1 mm
Head Rate	2.5 mm/min
Global Strain $\bar{\varepsilon}_y$	4.7%

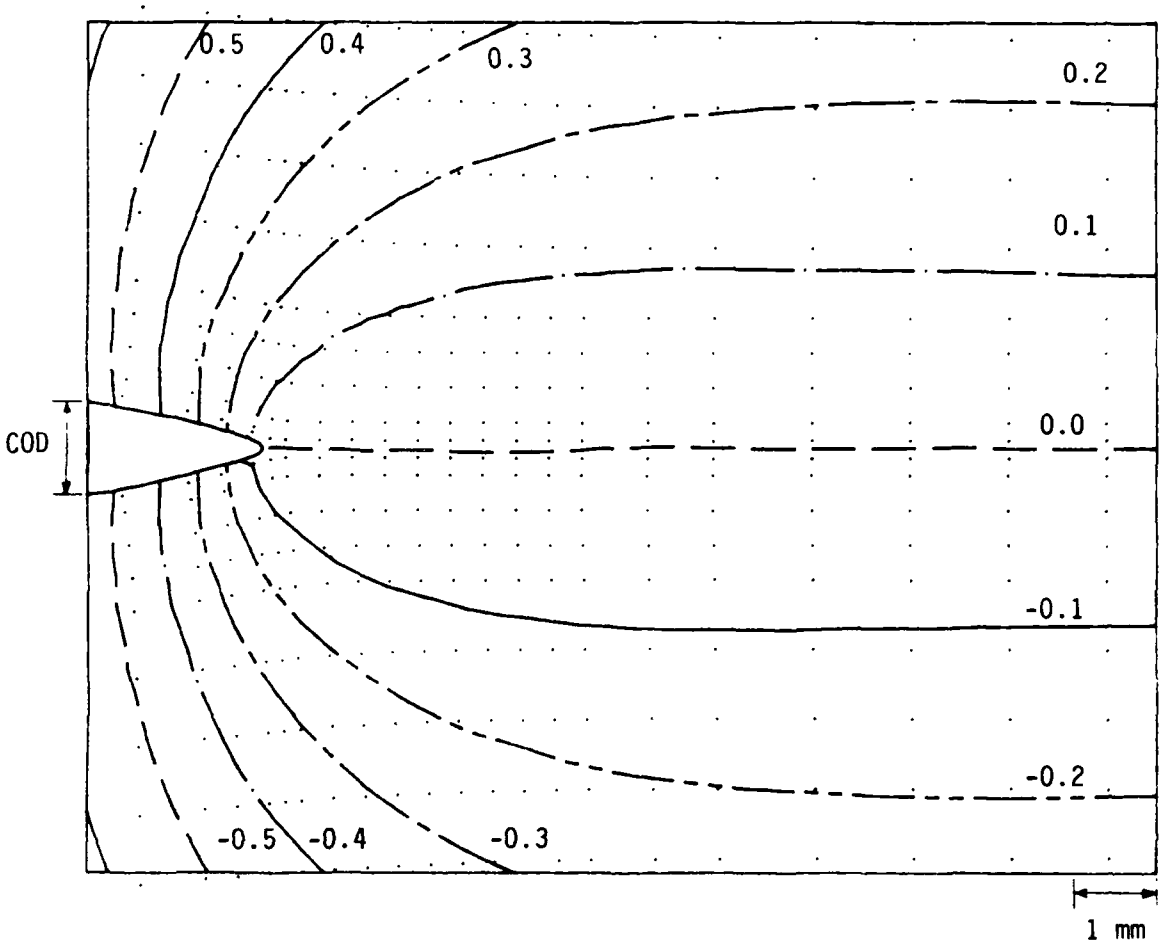

Fig. 5 g) V Displacement Field, Slow Rate, PB

Test	B5
Near Tip Field of Digitized Interval	ε_x 0.05
Head Rate	2.5 mm/min
Global Strain $\bar{\varepsilon}_y$	4.7%

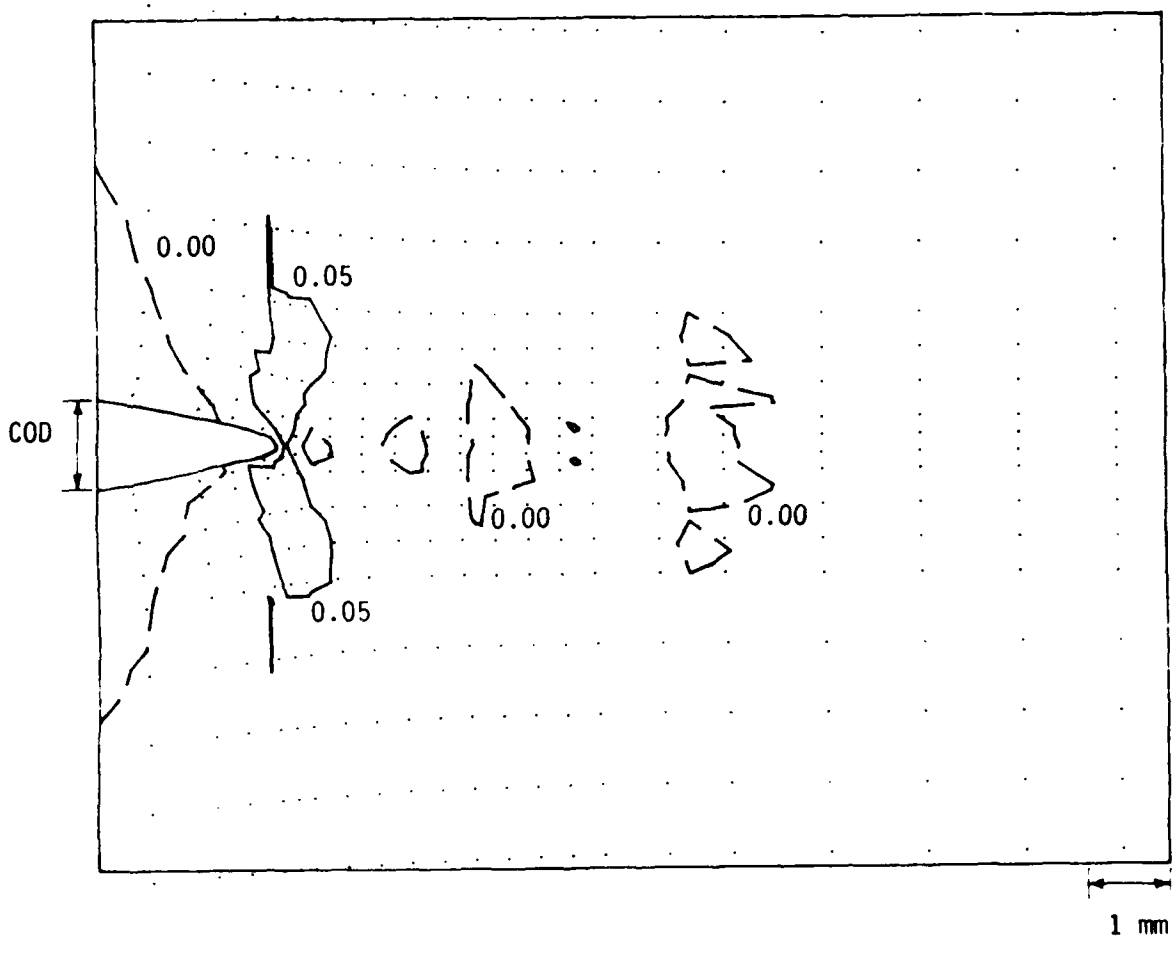

Fig. 5 h) ε_x Slow Rate, PB

Test	B5
Near Tip Field of Digitized Interval	ε_y 0.05
Head Rate	2.5 mm/min
Global Strain $\bar{\varepsilon}_y$	4.7%

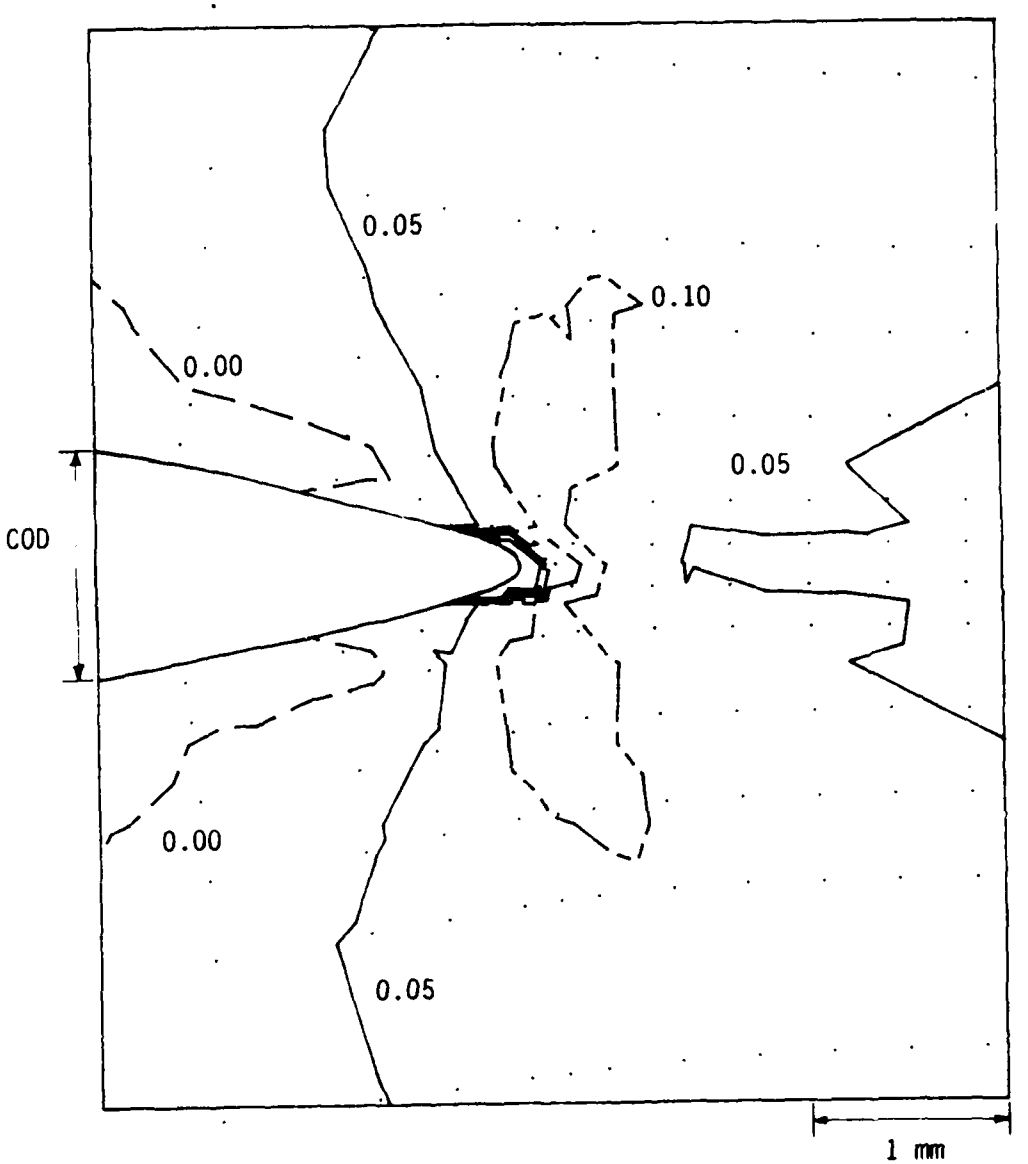

Fig. 5 i) ε_y Slow Rate, PB

Test	B5
Near Tip Field of Digitized Interval	γ_{xy} 0.05
Head Rate	2.5 mm/min
Global Strain $\bar{\varepsilon}_y$	4.7%

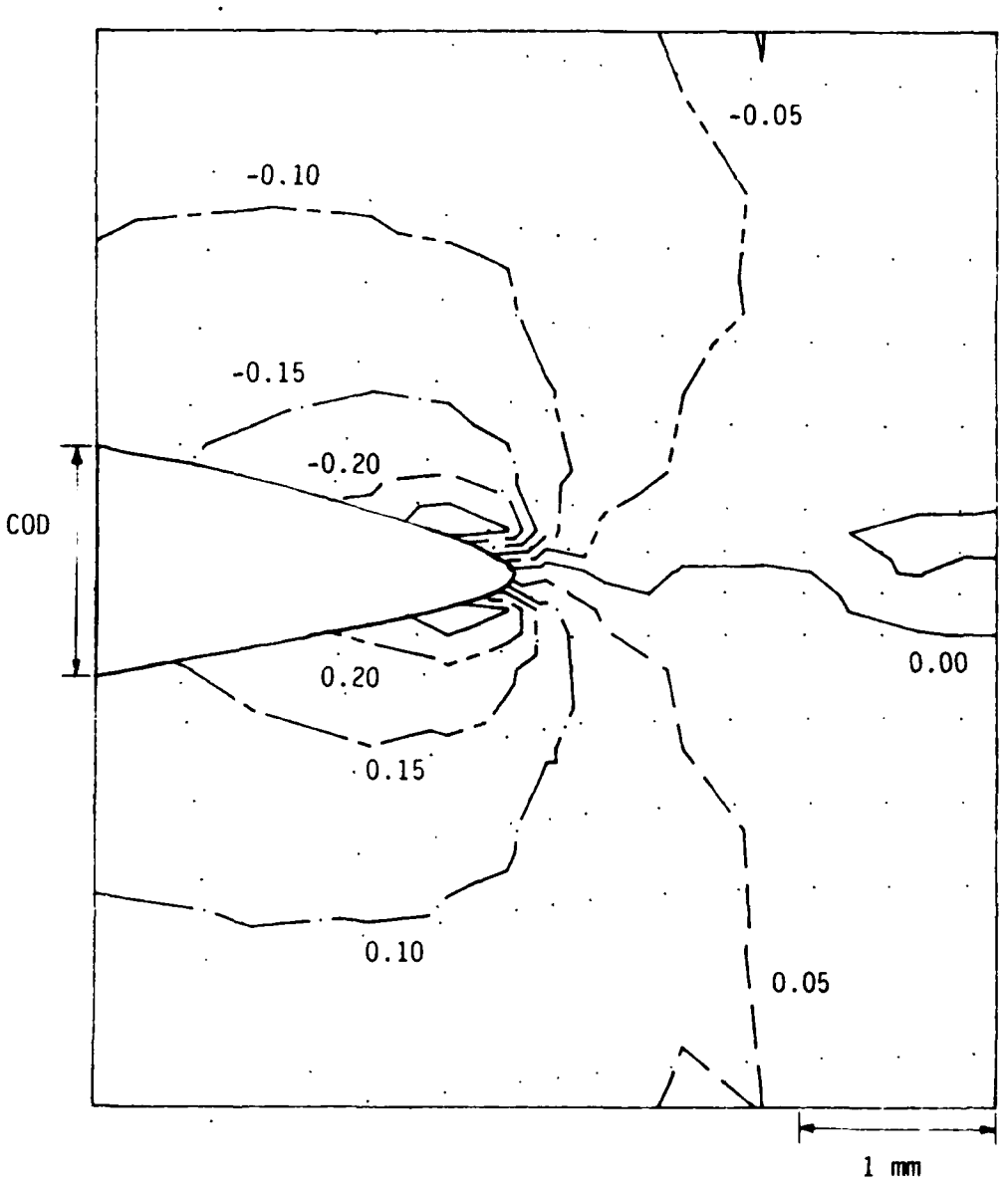

Fig. 5 j) γ_{xy} Slow Rate, PB

Figure 6 shows typical crack front shapes which were traced from dye markings on inert propellant and pure binder respectively. It is clear that there is no thumbnailing in the inert propellent specimen. This result was typical of all tests on the inert propellant and was somewhat unexpected. However, if one focuses upon the damage zone aneac of the crack, one may conjecture that resin rich tubes of binder which are formed here (see Figure 7) may not be strongly transversely connected, thus eliminating the transverse constraint normally associated (as a precursor) with thumbnailing. This is an important observation since, if true, it may mean that no plane strain fracture toughness will exist for this material in this environment.

The crack fronts displayed by the pure binder were even more remarkable. As seen in Figure 6, a small amount of reverse thumbnailing occurred. It was also noticed that crack growth may have been slightly retarded by the grating on the grating side. The reason for the inverse thumbnailing is not clear unless the surface of the very soft binder material could have been damaged in making the initial crack and this influenced the crack front shape which was only extended by about 2 mm.

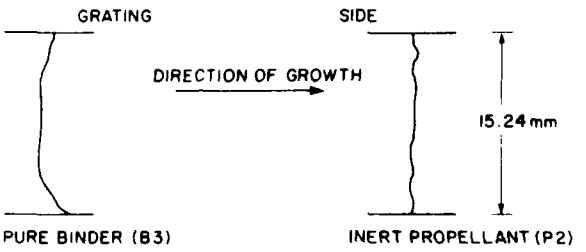

Fig. 6 Crack Border Shapes After Some Growth

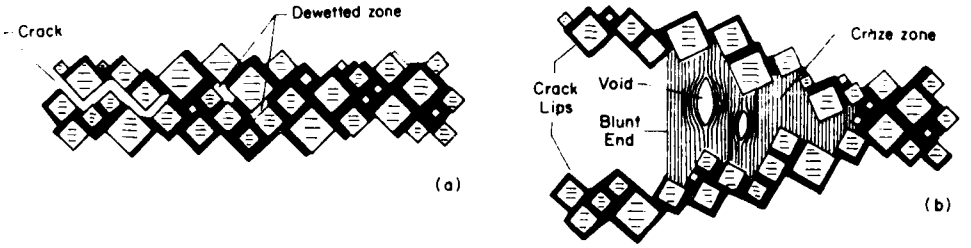

Fig. 7 Idealized Material Behavior During Crack Opening (large particles spearate, stretching the binder into tubes between which voids develop) (a) No Load, (b) Under Load

It was also observed that severe blunting occurred in the inert propellant (as noted in Ref. 1) leading to the use of a modified algorithm for use in extracting the lowest eigenvalue λ_u from the data in the form:

$$V-(V)_0 = D_y r^{\lambda_u} \qquad (1)$$

However, in the pure binder, the blunting was absent and $(V)_0 \approx 0$.

Figure 8 illustrates the use of the equation:

$$\ln[V-(V)_0] = \ln D_y + \lambda_u \ln r \qquad (2)$$

to determine λ_u. Results from the biaxial tests are shown in Table II.

TABLE 2 - Biaxial Test Results

Inert Prop. Tests

Test P1

Linear Zone (range) = 3.5-5.0 mm
Displ. Rate = 2.54 mm/min

ε%	λ_u	$2v_0$(mm)
1.5%	.629	.102
3.3%	.744	.476
4.8%	.532	.143
8.0%	.648	.344

λ_u(avg) = 0.638

Test P2

Linear Zone (range) = 1.5-5.0 mm
Displ. Rate = 2.54 mm/min

ε%	λ_u	$2v_0$(mm)
.76%	.642	0
2.75%	.674	.20
5.54%	.582	.16
7.57%	.652	.26
10.81%	.792	.13
24.05%	.712	0.0

λ_u(avg) = 0.676

Test P3

Linear Zone (range) = 1.5-4.5 mm
Displ. Rate = 25.4 mm/min

ε%	λ_u	$2v_0$(mm)
.79%	.592	.044
1.58%	.604	.136
3.16%	.619	.384
6.43%	.570	.247
10.38%	.567	.186
12.74%	.681	.144
13.54%	.741	.160

λ_u(avg) = 0.625

Test P4

Linear Zone (range) = 1.5-5.0 mm
Displ. Rate = 25.4 mm/min

ε%	λ_u	$2v_0$(mm)
1.67%	.643	0
5.64%	.646	.18
6.43%	.761	0
8.03%	.677	0
13.64%	.717	.08

λ_u(avg) = 0.689

TABLE 2 Biaxial Tests Results Continued

Pure Binder Tests

Test B1

Linear Zone (range) = 2.0-6.0 mm
Displ. Rate = 2.54 mm/min,
$2v_0$ = 0 mm

ε%	λ_u
1.94%	.727
3.49%	.628
5.06%	.569
6.60%	.597
9.74%	.568
17.35%	.597

λ_u(avg) = 0.614

Test B2

Linear Zone (range) = 1.5-5.0 mm
Displ. Rate = 2.54 mm/min,
$2v_0$ = 0 mm

ε%	λ_u
.37%	.748
1.93%	.730
3.47%	.737
12.87%	.631
17.36%	.670

λ_u(avg) = 0.703

Test B3

Linear Zone (range) = 1.0-6.0 mm
Displ. Rate = 25.4 mm/min,
$2v_0$ = 0 mm

ε%	λ_u
1.65%	.807
3.24%	.642
6.41%	.569
7.98%	.573
12.80%	.526
16.05%	.556

λ_u(avg) = 0.612

Test B4

Linear Zone (range) = 1.5-5.0 mm
Displ. Rate = 25.4 mm/min
$2v_0$ = 0 mm

ε%	λ_u
6.40%	.749
8.00%	.722
11.20%	.660
12.80%	.668

λ_u(avg) = .700

Test B5

Linear Zone (range) = 1.5-5.0 mm
Displ. Rate = 2.54 mm/min,
$2v_0$ = 0 mm

ε%	λ_u
4.68%	.595
6.24%	.587
7.80%	.580
12.52%	.534

λ_u(avg) = 0.574

Test B6

Linear Zone (range) = 1.5-5.0 mm
Displ. Rate = 2.54 mm,
$2v_0$ = 0 mm

ε%	λ_u
7.03%	.641
10.55%	.608
12.92%	.556
15.30%	.566
17.36%	.602

λ_u(avg) = 0.595

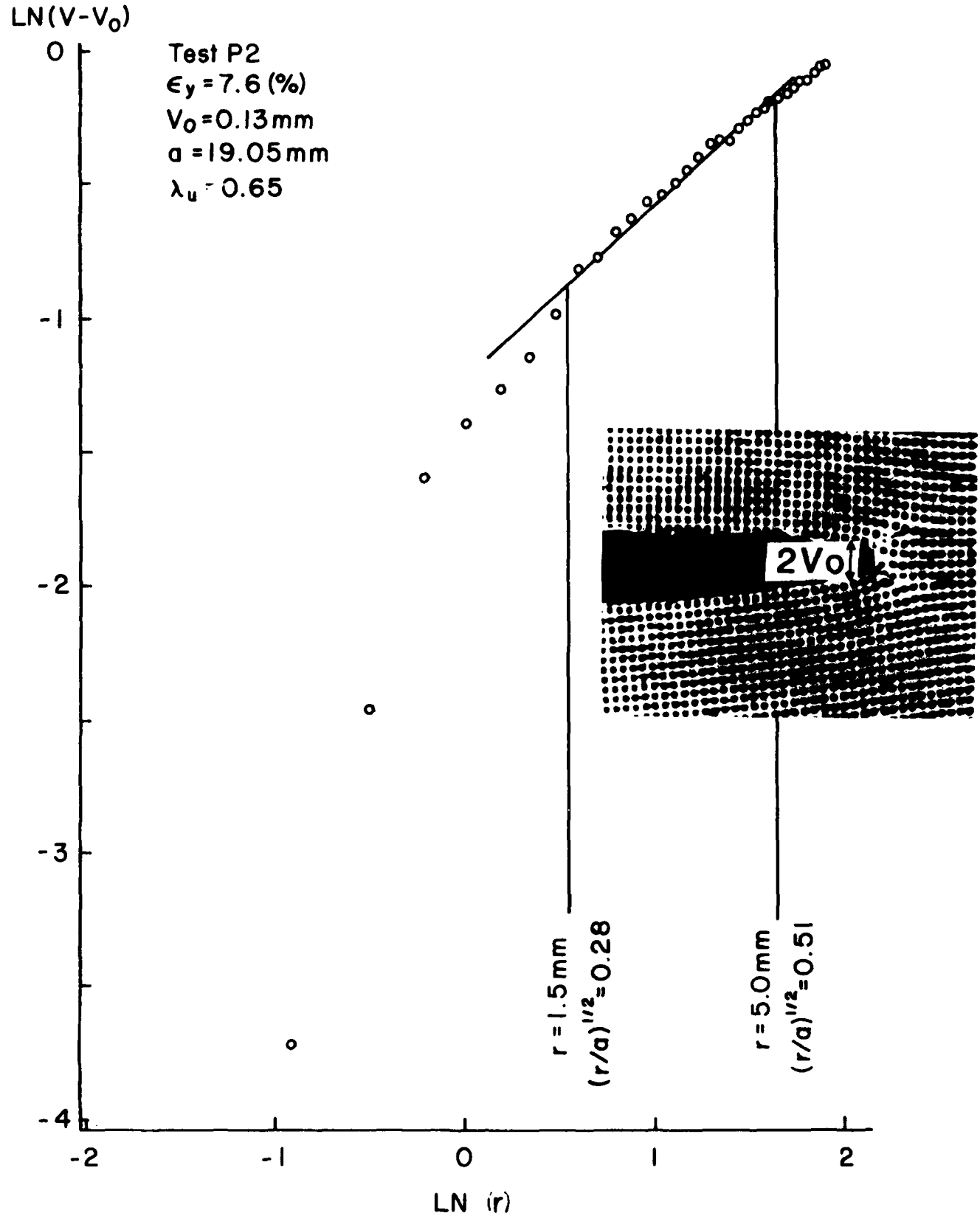

Fig. 8 Determination of λ_u from Inert Propellant Data

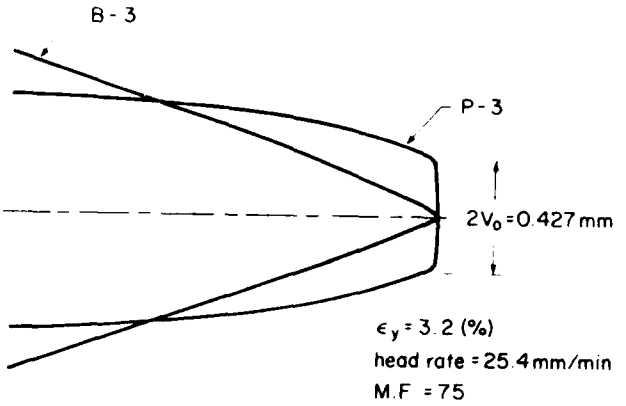

Fig. 9 Crack Tip Profiles for Inert Propellant and Pure Binder

The current results for the inert propellant yield values of λ_u at the free surface which are similar to those obtained in Ref. 1. However, the zone dominated by these values is further from the crack tip (0.5 to 1.5 mm in Ref. 1 vs. 1.5 to 5.0 mm) herein. The similarity in λ_u values would be expected since neither set of crack fronts were thumbnailed. The shift in the location of the zone where λ_u dominates is also expected since higher global strain levels (and more crack opening) were obtained during crack growth in the current experiments than in the measurements prior to crack growth in Ref. 1.

Another observation is that the zone dominated by λ_u was as far as or farther from the crack plane in the pure binder tests than in the current inert propellant tests even though $V_0 \approx 0$ in the former tests. This is believed due to the larger crack opening in the binder tests as illustrated in Figure 9. The rather large scatter in the λ_u values from the binder tests is likely partially due to the effect of the reverse thumbnailing which caused the angle of intersection between the free surface and the crack border to differ significantly from 90°.

There was a noticeable difference in the crack growth process observed in Ref. 1 and that observed in the inert propellant in the current program. In the tests reported in Ref. 1, the crack extended by first blunting extensively and then connecting with one or more voids above or below the original crack plane, producing an undulating or meandering path about the original crack plane. In the current tests the blunting, although still present, was much less than in Ref. 1. This appeared to focus the high strain zone ahead of the crack closer to the original crack plane, and resulted in elimination of the meandering effect. This is described pictorially in Figure 10. The severe blunting in Ref. 1 is conjectured to be due primarily to resin rich layers of material on the free surfaces of the specimen which were absent from the current program.

FROZEN STRESS TESTS

Since thumbnailing did not occur along the crack front in the biaxial tests on the inert propellant, the frozen stress data for estimating the variation of λ_u with thickness were taken from four point bend tests on straight front cracks in a stress freezing epoxy material.

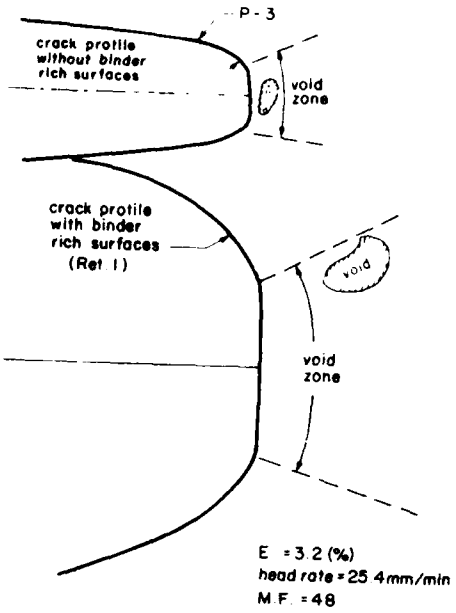

Fig. 10 Explanation of Difference in Crack Growth Features Between Results of Ref. 1 and Current Experiments. (Profiles prior to growth)

The specimen dimensions are given in Figure 11. A companion test series employing naturally grown cracks which did thumbnail was also conducted.

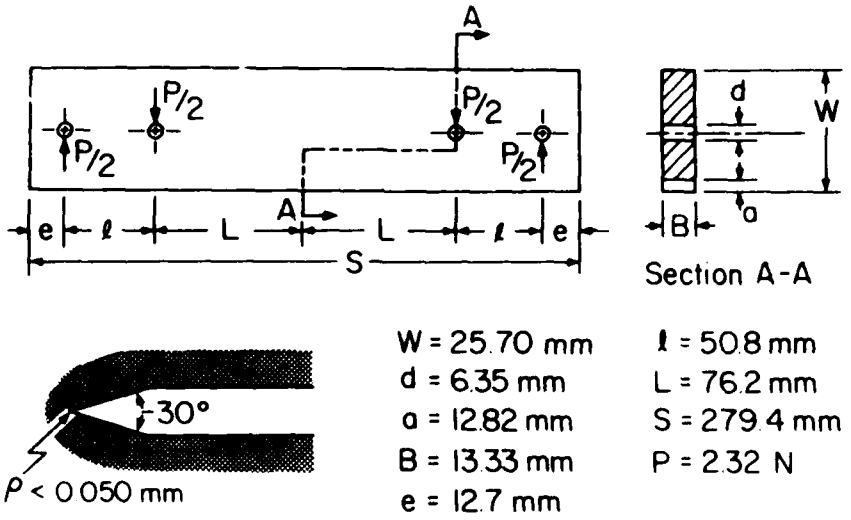

Fig. 11 Four Point Bend Specimen Dimensions

All such specimens were prepared from stress free di-phase transparent epoxy plates. Fairly dense moire gratings (600 and 1200 lines/mm 1.75×10^{-2} mm thick) were cemented to the free surface in the neighborhood of the point of intersection of the crack front with the free surface and the specimens were then placed in a cam-controlled oven and heated to critical temperature (≈ 225°F or 107°C). After a thermal soak, four point loads were applied, and the natural cracks were grown to desired size. After cooling under load, specimens were removed from the oven and the deformed gratings at the free surface were viewed through a master virtual grating which was made by splitting a laser beam and reflecting one part back into the path of the other part to form walls of constructive and destructive interference. This virtual grating was tuned to twice the frequency of the active grating on the

specimen surface with a diffraction grating. A typical moire pattern for the displacement component normal to the tip of a thumbnailed crack is shown in Figure 12. After obtaining λ_u from this pattern using Eq. 2 (with $V_0 = 0$), slices were removed mutually orthogonal to the crack front and the crack plane, and analyzed photoelastically. Using the variable λ algorithm described in Appendix B (Eq. B-7), values for λ_σ^* were obtained through the thickness of the specimens. Figure 13 compares the distributions of λ_σ for the straight front and thumbnailed cracks. The λ_σ distributions from two thumbnailed cracks whose crack fronts are also shown in Fig. 13 are superimposed on the distribution for two straight front cracks, the latter results taken from Ref. 1. Considering the inevitable data scatter present in such data, one concludes that any differences between the two data sets appear to be of the order of the data scatter itself. Part of the scatter may be due to lack of symmetry of the natural cracks but no adjustments in the data were made to account for this effect.

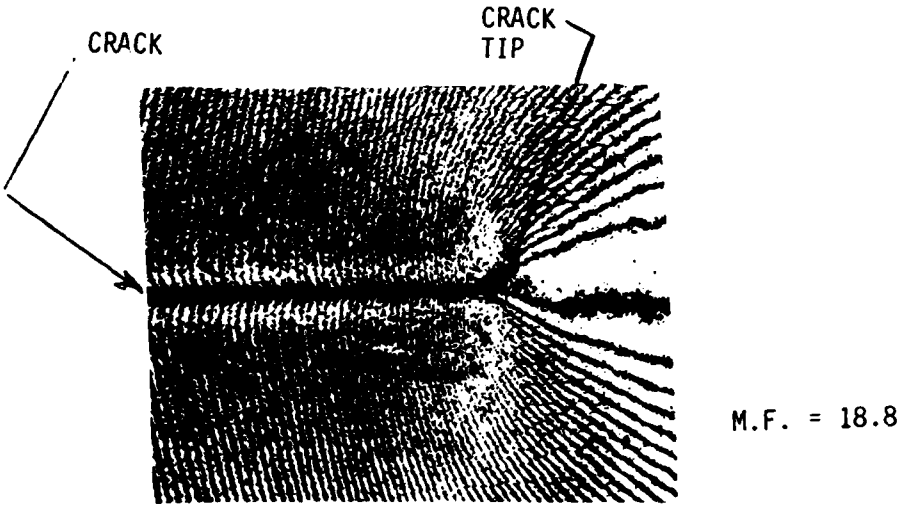

Fig. 12 Moire Pattern for Near Tip Displacement Field (V) at Free Surface of Inert Propellant Containing a Natural Crack

Figure 14 shows a comparison between the normalized K_1 distributions for the straight front and natural cracks computed from Eq. (B-4) in Appendix B. The "hump" in the K_1 distribution for the thumbnailed cracks occurs near where the curvature of the thumbnailed cracks reverses and may be related to that event (marked with tick marks in Fig. 13). Moreover, growth of the thumbnailed cracks was not symmetrical. Slices were taken both parallel to the free surface and normal to the crack front. While the values of K_1 were always higher for slices taken normal to the crack front (as expected), there was less data

* $\lambda_u = 1 - \lambda_\sigma$

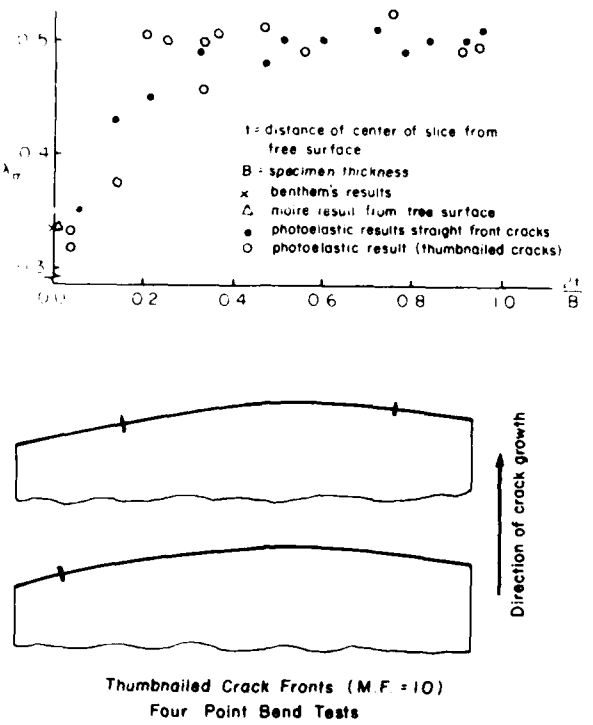

Fig. 13 λ_σ Distributions for Straight Front and Thumbnailed Cracks

scatter in the slices taken parallel to the free surface. Both slicing methods, however, revealed the hump in the K_1 distribution. Near the hump, scatter was of the order of ± 6%. Although part of this scatter could be due to optical and material noise, it is more likely the result of crack front curvature which was not symmetrical with respect to the center of the thickness.

SUMMARY

Optical methods which exert negligible influence on near tip behavior of both inert propellant and pure binder in through cracked bodies were used to measure the displacement fields on the free surface of biaxial test specimens in the neighborhood of the crack front-free surface intersection point under Mode I loading at head rates differing by an order of magnitude. For this purpose, grating methods were employed. Data collected were digitized and surface in-plane displacement and strain fields were plotted. The value of the dominant eigenvalue λ_u at the free surface was extracted from the displacement field measurements.

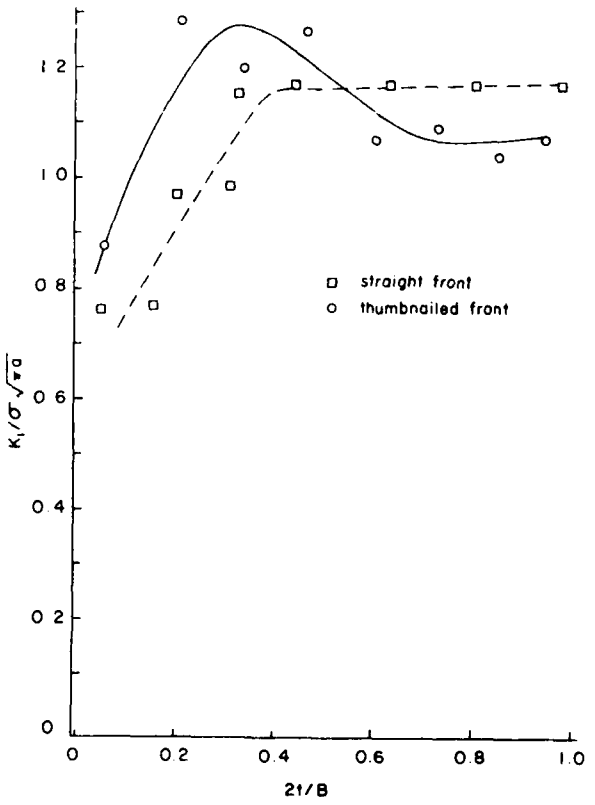

Fig. 14 Stress Intensity Factor Distributions in Four Point Bend Specimens with Straight and Thumbnailed Crack Fronts

Using the results from high density moire interferometry and frozen stress analysis of four point bend specimens of di-phase photoelastic materials, the distribution of λ_u through the thickness was inferred for both straight front and "thumbnailed" cracks.

The studies described above together with those of Ref. 1 lead to the following observations and conclusions regarding near tip behavior of inert propellant in cracked biaxial specimens under Mode I loading.

OBSERVATIONS AND CONCLUSIONS

The crack extension process in inert propellant consists of two phases; firstly, crack opening and blunting during which severe stretching of the binder material ahead of the crack produces a binder-rich craze-like zone of binder tubes containing voids (Fig. 7) ahead of the crack. The blunting phase is due to the presence of the rigid particles

of inert propellant and did not occur in tests on pure binder. The direction of crack extension may oscillate about the plane of the main crack if excess binder is present (Fig. 10).

When the cracks grow in inert propellant, the crack front remains straight, indicating an absence of transverse constraint in the craze zone ahead of the crack. This is an important observation, since it means that a plane strain fracture toughness may not exist for this material at room temperature.

Values of the lowest dominant eigenvalue λ_u can be accurately measured at the free surface of the inert propellant provided the influence of blunting is properly accounted for in the algorithm for the displacement field (Eq. 2).

The four point bend test results appear to yield a good description of the variation of λ_u from its free surface value back to the value of one half as per LEFM (Fig. 13).

Changing the crosshead speed from 2.5 to 25.4 mm/min. altered the displacement and strain fields significantly but not the global contour patterns or values of λ_u.

When compared to results from cracked test specimens of pure binder, the main influence of the rigid particles in IP on near tip behavior is to enlarge an intense zone of normal strain normal to the crack plane to a size at least an order of magnitude greater than its size in cracked specimens of pure binder. This, in turn, enlarges the surrounding strain fields (Fig. 5). The rigid particles also served to strengthen and stiffen the material globally (Fig. 3).

REFERENCES

[1] Post, D., Smith, C. W. and Czarnek, R., Crack Opening and Extension in Inert Solid Propellant; An Experimental Study, AFAL-TR-87-043, VPI&SU, Blacksburg, Va., Sept. 1987.

APPENDIX A

DIGITIZATION PROCESS

Points located at the intersection of the grating lines (such as those shown in Fig. 4) are selected close together in regions of expected high gradients and further apart away from these regions. These points in groups of four form quadrilaterals (initially rectangular) and values are read at each of four points and averaged before and after loading. The four point average is located at the centroid of each quadrilateral and the difference between the no-load and loaded values becomes the digitized displacement at that point. An array of these latter points before and after loading are shown in Figs. A-1 and A-2 along with the corresponding displacement contours plotted by computer. The computer program plots contours representing the displacements of the points from their initial positions (Fig. A-1) to their final positions (Fig. A-2).

Test	P2
Near Tip Field of	V
Digitized Interval	0.1 mm
Head Rate	2.5 mm/min
Global Strain $\bar{\varepsilon}_y$	4.0 %

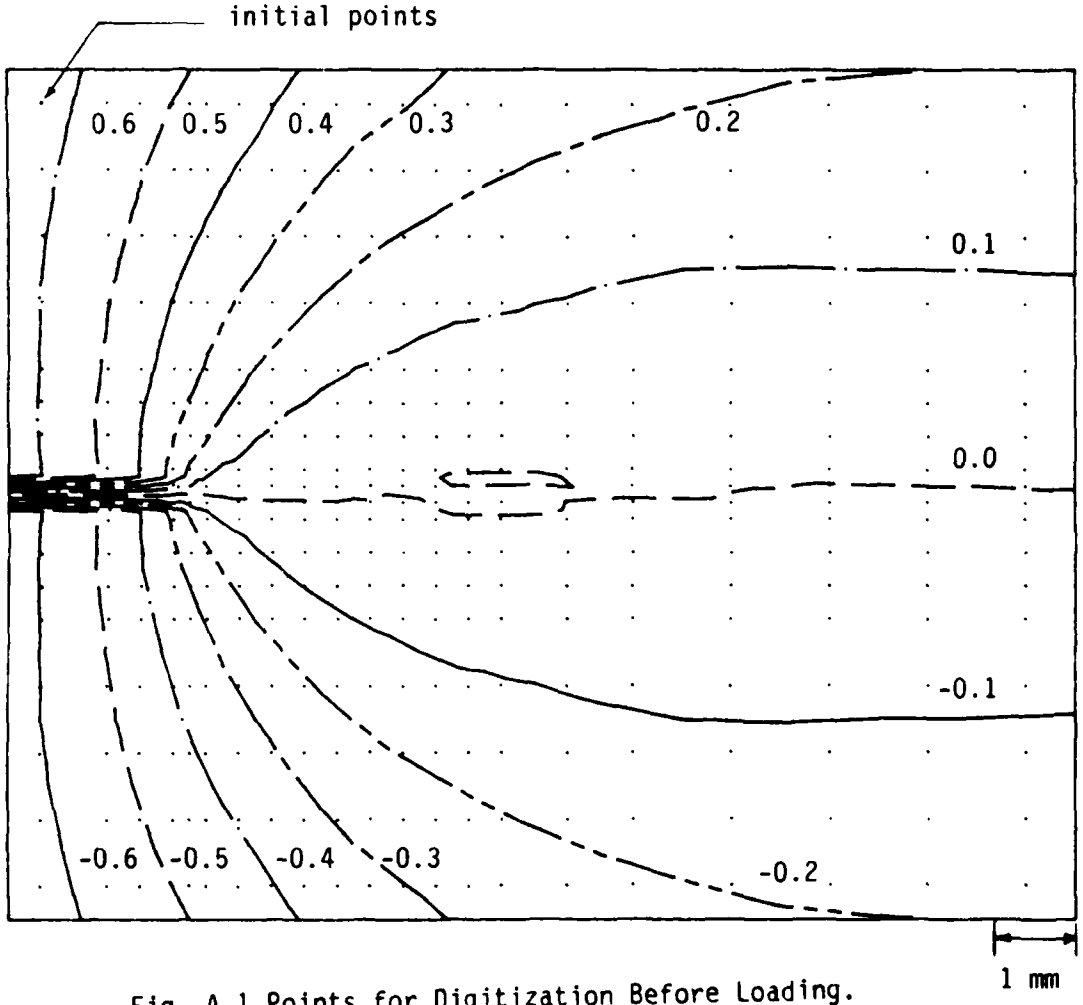

Fig. A-1 Points for Digitization Before Loading.

Test	P2
Near Tip Field of Digitized Interval	V 0.1 mm
Head Rate	2.5 mm/min
Global Strain $\bar{\varepsilon}_y$	4.0 %

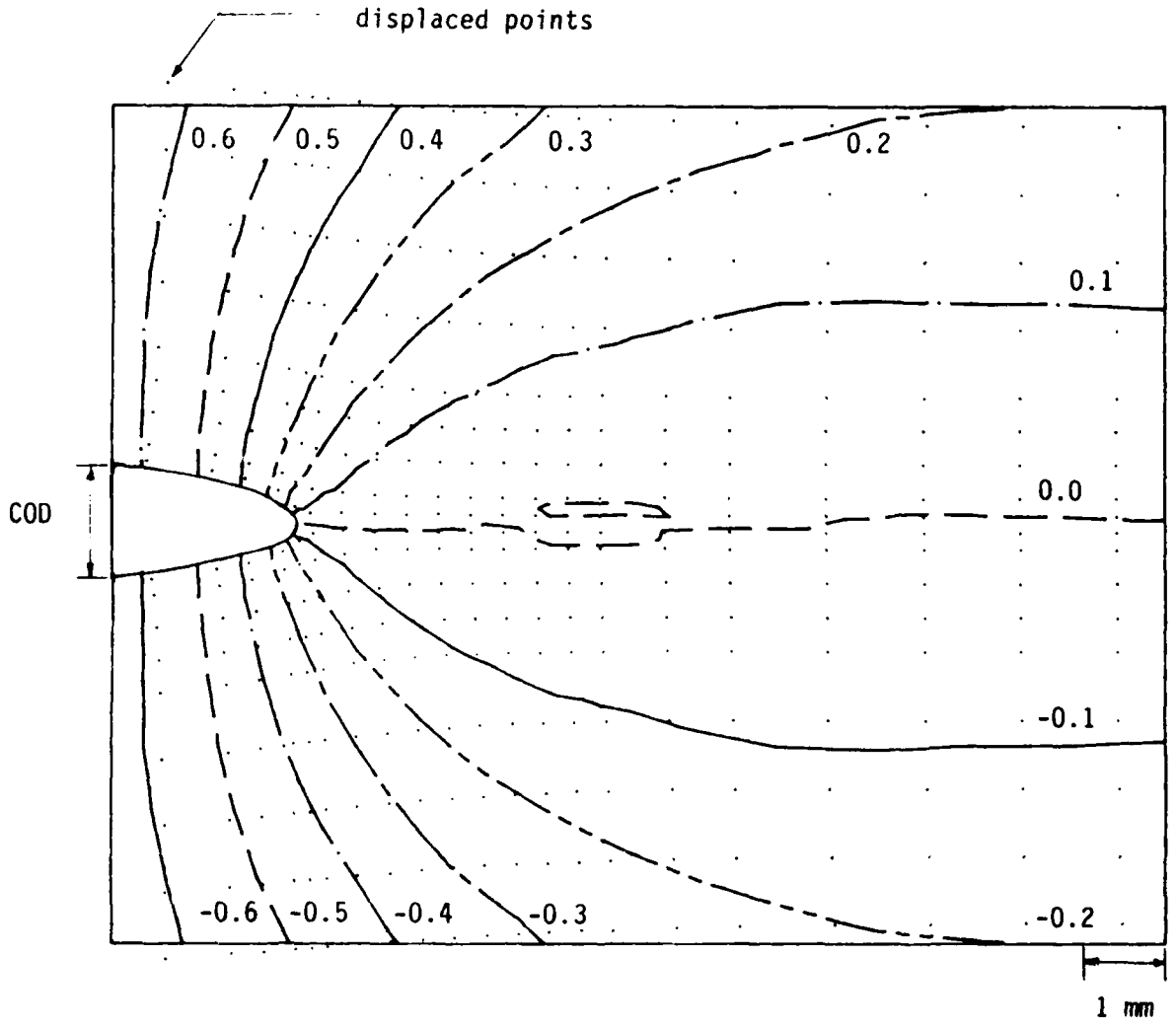

Fig. A-2 Points for Digitization After Loading.

APPENDIX B

LEFM FROZEN STRESS ALGORITHM - TWO PARAMETER APPROACH

By choosing a data zone sufficiently close to the crack tip that a Taylor Series Expansion of the non-singular stresses can be truncated to the leading terms, one may write for a straight front crack [B-1]

$$\sigma_{ij} = \frac{K_1}{(2\pi r)^{1/2}} f_{ij}(\theta) - \sigma^0_{ij}(\theta) , \quad i,j = 1,2 \qquad \text{(B-1)}$$

where σ_{ij} are the stress components in the x_1x_2 plane normal to the crack border, K_1 is the Mode I Stress Intensity Factor and r, θ are the polar coordinates with origin at the crack tip (see Fig. B-1). Along $\theta = \pi/2$, one has, for case where $(\sigma^0)^2$ is small relative to $8\tau^2_m$ (see Ref. [B-1] (where σ^0 is proportional to the contribution of the nonsingular stress to the maximum shear stress, τ_{max} in the x_1x_2 plane)

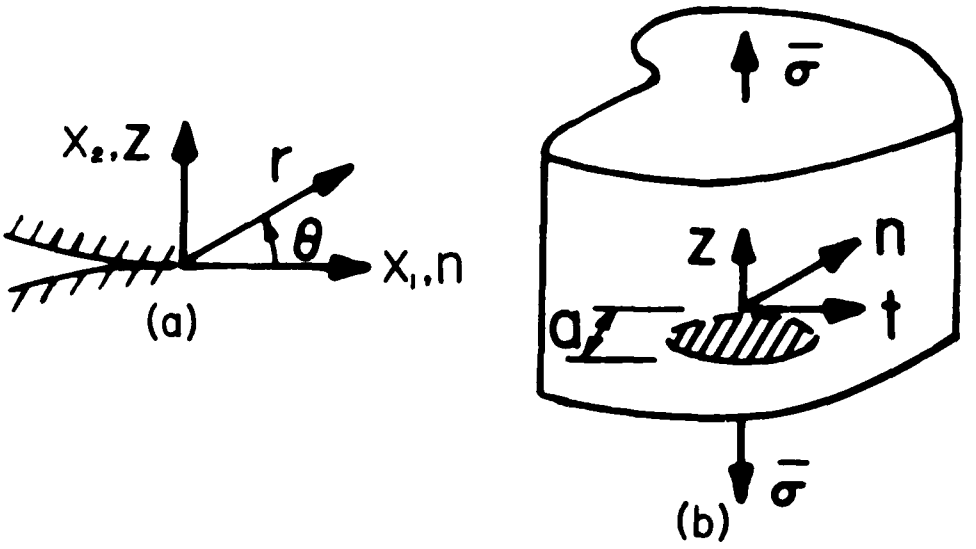

Fig. B-1 General Problem Geometry and Notation

$$\tau_{max} = \frac{K_1}{(8\pi r)^{1/2}} + \frac{\sigma^0}{\sqrt{8}} \qquad \text{(B-2)}$$

Now defining an "apparent" SIF,

$$K_{AP} = \tau_{max}(8\pi r)^{1/2} \qquad \text{(B-3)}$$

and normalizing with respect to $\bar{\sigma}(\pi a)^{1/2}$ where $\bar{\sigma}$ represents the remote stress and a the crack length, one has

$$\frac{K_{Ap}}{\bar{\sigma}(\pi a)^{1/2}} = \frac{K_1}{\bar{\sigma}(\pi a)^{1/2}} + \frac{\sigma^0}{\bar{\sigma}} \left(\frac{r}{a}\right)^{1/2} \qquad \text{(B-4)}$$

which suggests an elastic linear zone (ELZ) in a plot of $\frac{K_{Ap}}{\bar{\sigma}(\pi a)^{1/2}}$ vs $\left(\frac{r}{a}\right)^{1/2}$ with a slope of $\frac{\sigma^0}{\bar{\sigma}}$. Experience shows this zone to lie between $(r/a)^{1/2}$ values of approximately 0.2 to 0.4 (or above) in two dimensional problems. By extracting optical data from this zone and extrapolating across a near tip nonlinear zone, an accurate estimate of $K_1/\bar{\sigma}(\pi a)^{1/2}$ can be obtained. This is illustrated in Figure [B-2] for two slices at different locations in a four point bend specimen. This approach may be directly extended to 3D problems involving curved crack fronts by replacing i,j values of 1,2 by n,z where the nz plane is normal to the crack border at each point along the flaw border and the n,z,t coordinate system is a local cartesian system which follows the crack border (Figure B-1). In three dimensional problems the outer boundary of the data zone is usually restricted to $(r/a)^{1/2} \approx 0.4$ or less.

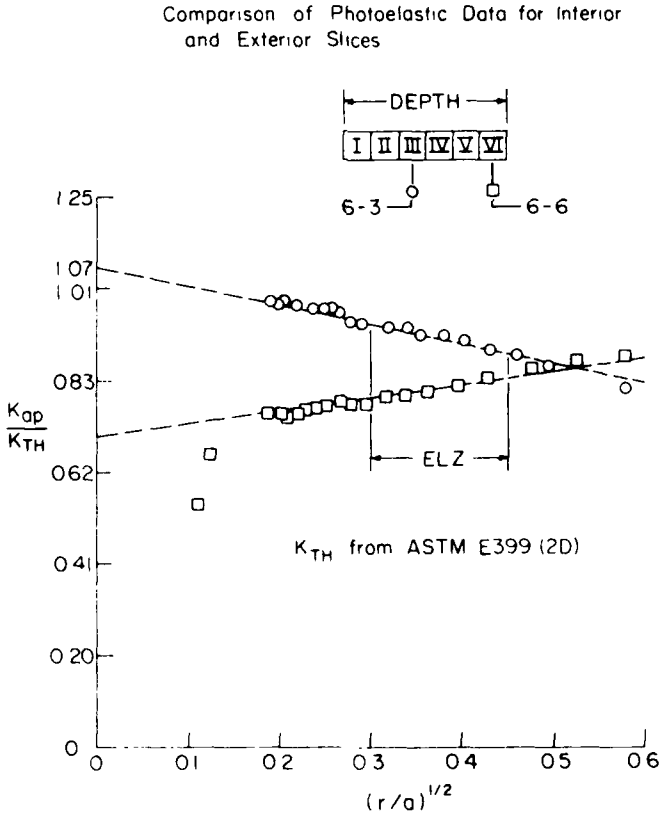

Fig. B-2 Determination of Stress Intensity Factors from Frozen Slice Data in Four Point Bend Specimen

VARIABLE λ_σ ALGORITHM

Following the above approach and the work of Benthem Ref. [B-2], one may formulate an expression for the near tip σ_{ij} in the form:

$$\sigma_{ij} = \frac{F_{ij}(\lambda_\sigma, \theta)}{r^{\lambda_\sigma}} - \sigma^0_{ij} \quad (i,j = n,z) \tag{B-5}$$

where $\sigma^0_{ij} = \sigma^0$ for i,j = n and zero for all other values of i,j. From Eqs. (B-5) one may develop an algorithm from which values of λ_σ may be extracted but the procedure is not as straightforward due to the presence of the second term in Eq. B-5 and the highly three dimensional nature of the near tip stress state at the free surface. If one evaluates τ_{max} from Eq. (B-5) along $\theta = \pi/2$ as done in LEFM, one obtains:

$$\tau^{nz}_{max} = \frac{\lambda_\sigma K_{\lambda_\sigma}}{\sqrt{2\pi}\, r^{\lambda}} + \frac{\sigma^0}{2} \sin(\lambda_0 + 1)\frac{\pi}{2} = \lambda_\sigma \frac{(K_{\lambda_\sigma})_{Ap}}{\sqrt{2\pi}\, r^{\lambda}} \tag{B-6}$$

where K_{λ_σ} may be designated a stress eigenfactor. Defining $\tau^*_0 = \frac{\sigma^0}{2} \sin(\lambda_\sigma + 1)\frac{\pi}{2}$, one obtains

$$\ln(\tau^{nz}_{max} - \tau_0) = \ln\left\{\frac{\lambda_\sigma K_{\lambda_\sigma}}{\sqrt{2\pi}}\right\} - \lambda_\sigma \{\ln r\} \tag{B-7}$$

REFERENCES

[B-1] Smith, C. W., "Use of Three Dimensional Photoelasticity and Progress in Related Areas", Experimental Techniques in Fracture Mechanics 2, Society for Experimental Mechanics, Bethel, Ct., pp. 3-58 (1975).

[B-2] Benthem, J. P., "The Quarter-Infinite Crack in a Half Space; Alternative and Additional Solutions," Int. J. of Solids & Structures, Vol. 16, pp. 119-130 (1980).

* τ_0 is first computed from LEFM at all points (i.e. using $\lambda_\sigma = 1/2$) except at the free surface where we set $\tau_0 = 0$. Then, at the onset of decreasing τ_0 below midthickness values, we decrease τ_0 linearly from that point to zero at the free surface. This approach adequately accounts for the effect of the nonsingular stress.